Seismic analysis of high-rise mega-braced frame-core buildings

CrossMark

E. Brunesi *, R. Nascimbene [1], L. Casagrande [2]

EUCENTRE, European Centre for Training and Research in Earthquake Engineering, Via Ferrata 1, 27100 Pavia, Italy

A B S T R A C T

This work summarizes the results of a series of nonlinear dynamic finite element analyses devoted to assess peculiar aspects in the seismic response of high-rise mega-frame prototypes with outriggers and belt trusses. Thirty- and sixty-storey planar frames, extracted from reference three-dimensional structures composed of an internal symmetric braced core, were designed in accordance with European rules. The core consisted of a concentrically braced frame system, while outriggers were placed every fifteen stories to limit inter-storey drifts and second order effects. Numerical models able to account for material and geometric nonlinearities were developed within an open source platform, using inelastic force-based fibre elements to model structural members and mechanical idealizations to reproduce the behaviour of bolted beam–column and welded gusset-plate connections. Out-of-plane imperfections were explicitly included in the braces to allow for potential buckling mechanisms in both braces and gusset plates.

Nonlinear time history analyses (NLTHAs) were performed, in comparison with response spectrum analysis (RSA), aiming to quantify the potential of such systems, when included in the lateral-force resisting system of modern high-rise moment resisting frames (MRFs). Global and local performance were investigated in terms of inter-storey drift and acceleration peak profiles, shear and bending moment demands, as well as axial force–displacement curves and static-to-seismic load ratios in critical braces at different floor levels. Sensitivity to the structure height was explored comparing the responses of the two prototypes. Trends were discussed to show that, if accurately designed and detailed in light of capacity design principles and performance-based design concepts, these systems provide an optimum combination of stiffness and strength.

© 2016 Elsevier Ltd. All rights reserved.

1. Introduction

The growing use of high-strength materials and advanced construction techniques, in combination with urbanization needs, has led a significant increase in the number and variety of high-rise structures, causing these super-tall buildings with mega-frame systems to have a larger and larger impact on economy and society [1–3]. Such modern and more flexible buildings have complicated structural systems consisting of hundreds of different components, including those with complex features and large dimensions [4–7], and their increasing height poses challenges for seismic design in terms of stiffness, strength and stability, particularly in areas of high seismicity. When compared to medium- and low-rise build-ings, tall mega-braced frame systems present several distinctive characteristics in their behaviour and peculiar aspects in their design, such as long periods and higher mode effects [1–15]. If strength criteria are usually dominant factors in the design of low-rise structures, stiffness and stability may often govern the design process when building height increases. To ensure safe and economic design, construction and operation under various extreme loading conditions in particular during earthquake events, detailed studies are required to predict their response, being the majority of current seismic Standards often unsuitable for them [16–18]. In addition, scaled shaking table tests [19,20] are at the moment promising analysis techniques for research applications but they are not so easily applicable for design office use. Therefore, high-definition or simplified finite element (FE) idealizations still represent an attractive tool to explore the seismic performance of these complex structural systems, as shown by a number of research efforts available in literature on that subject [1–15]. If early studies [9–15] introduced simplifications in either numerical modelling or analysis technique, significant improvements have been more recently achieved [1–8].

* Corresponding author. Tel.: +39 0382 5169893; fax: +39 0382 529131.
E-mail addresses: emanuele.brunesi@eucentre.it (E. Brunesi), roberto.nascimbene@eucentre.it (R. Nascimbene), lorenzo.casagrande@eucentre.it (L. Casagrande).
[1] Tel.: +39 0382 5169827; fax: +39 0382 529131.
[2] Tel.: +39 0382 5169903; fax: +39 0382 529131.

Generalized hand-methods [11] and highly efficient random vibration algorithms [10] have been developed to investigate the dynamic properties of irregular high-rise systems in linear fashion. Classical lumped-plasticity approaches [9,13–15] have been extensively examined to propose pushover procedures for seismic response assessment of tall buildings. Simplified lumped-parameter analytical models, developed along the lines of equivalent single- or multiple-vertical-line-element solutions [12] have been integrated in an analytical framework for seismic fragility analysis of high-rise structures. Different design strategies, prepared according to stiffness- and strength-based criteria, have been discussed for diagrid and secondary bracing systems [4–7] using the results of static analyses, with and without P-Δ effects, which were carried out under factored gravity and wind loads. In these studies [4–7], linear elastic simulations were conservatively performed assuming beam-to-column joints and diagonal-to-diagonal connections to behave as perfectly pinned systems. "Ad hoc" constitutive laws for concrete filled steel tube columns of super-tall buildings have been validated by experimental observations and then implemented in more refined fibre-beam and multi-layer shell models [1–3] using general-purpose commercial FE codes.

In light of this scenario, the present paper details and discusses a modelling procedure for large scale implicit nonlinear dynamic simulation of mega-frame systems composed of a concentrically braced frame (CBF) core and outriggers/belt trusses which are combined to resist vertical and earthquake-induced lateral loads. To this aim, this study combines the force-based fibre element [21,22] with the open FE platform OpenSees [23], integrating detailed modelling approaches able to reproduce the cyclic behaviour of key structural components, such as bolted and gusset-plate connection systems, in a geometrically and materially nonlinear transient dynamic analysis. First, two reference prototypes, the prevailing geometric characteristics of which are summarized in the following, have been designed in medium ductility class (DCM) according to current European prescriptions (i.e. EC8 [24]), using response spectrum analysis (RSA), and then fibre-based FE models have been prepared to examine their nonlinear dynamic behaviour, using a set of natural ground motions scaled to obtain displacement spectrum compatibility in accordance with EC8 requirements [25,26]. Hence, global inter-storey drift and acceleration peak profiles, as well as shear and bending moment demands, are collected and their average is compared with the results determined by RSA in order to highlight design criticalities in current seismic Code provisions [24], when applied to flexible high-rise structures specifically designed for medium/low dissipative behaviour. Finally, the local response of these two case-study buildings is discussed in terms of hysteretic behaviour of critical braces and peak compressive loads experienced by the outriggers during nonlinear time history analyses (NLTHAs). This study will serve as a reference for earthquake-resistance design/analysis of super-tall buildings of similar type.

2. Structural nonlinear dynamic analysis

Nonlinear response history analysis is a robust and effective tool to dynamically determine seismic demands, as well as to identify plastic hinge mechanisms in structures. Conversely, pushover analysis suffers from several inherent deficiencies and limitations [27,28] (e.g. invariant load distribution in traditional approaches, inability to safely account for higher-mode effects in more recent modal or multimodal adaptive solution procedures [28–31], uncertainties in the combination of different modal contributions, underestimates of plastic rotations in hinged sections [29,31,32]). As a result, nonlinear dynamic analysis has currently become a

favourite technique for building evaluation and design verification of high-rise moment resisting frames (MRFs) [1–3], with rapid developments in computer technology and computational algorithms.

Even though detailed brick- or shell-based FE models, commonly used in seismic analysis of steel and reinforced concrete structural systems and components [33–42], give more insight than equivalent mechanical idealizations, being able to reproduce their local response in terms of stress/strain concentrations, the computational time increases tremendously, requiring necessarily to take advantage of parallel processing on multiprocessor computers. Despite its accuracy and multipurpose potential, a detailed approach, using conventional 3D or 2D elements [33–42] or advanced beam/plate theories [43–54], is currently almost unfeasible if the response of an entire mega-frame system has to be investigated, particularly in a dynamic fashion. Higher-order formulations or onerous and complex meshes, consisting of 2D or 3D elements combined with contact or interface algorithms, are able to simultaneously account for many interacting sources of nonlinearity (e.g. plasticity, instability, slippage and thermomechanical coupling) in a phenomenological sense, but they imply a high level of complexity and computational effort.

By contrast, the complex contribution of bolted [35–38,55–57] and welded [33,34,58,59] joint systems can be easily incorporated into classical fibre force-based [60] FE models, able to represent the interaction amongst connection components in an equivalent manner. Therefore, mechanical representations have been assumed in this research to include global response and potential failure mechanisms of these widely used systems, as discussed later on. In particular, the prevailing assumptions concerning modelling approach and simulation techniques will be given in the following, after a brief description of main geometric characteristics and mechanical properties of the thirty- and sixty-storey planar frames examined. Finally, details of the seismic input selected to perform the series of NLTHAs and RSAs, the results of which are shown in the following section, will be provided.

2.1. Description of case-study structures

The two prototype thirty- and sixty-storey 6 × 6-bay buildings analyzed in this work, namely HR-01 and HR-02, are extracted from reference three-dimensional structures designed for high seismicity (i.e. PGA = 0.40 g) in accordance with current European seismic prescriptions [24]. Soil class C (i.e. 180 m/s < V_s < 360 m/s) is assumed to perform the design by a series of RSAs on three-dimensional models (see Fig. 1), including vertical seismic component, second order effects and accidental eccentricity of the seismic masses. SAP 2000 program [61] is used in the initial analysis and design of the two buildings. As depicted in Fig. 2, where a schematic of plan and elevation is provided, the lateral-force resisting system (LFRS) of each high-rise mega-braced frame-core building consists of an internal CBF core, with outriggers placed every fifteen stories in order to limit inter-storey drifts and second order effects. The central 16 × 16 m braced core is symmetrically arranged in both longitudinal and transverse directions and it is connected to HD columns via one-storey high belt-trusses consisting of in-floor braces and vertical trusses. Hence, this hybrid dual system, composed of bracing, outriggers, and belts, provides lateral stability, redistribute loads if some members are damaged by unforeseen circumstances and maximizes the spaces inside the building. Medium ductility class (DCM) according to EC8 provisions [24] is considered to carry out the design process and the behaviour factor (q) selected for V bracing systems is conservatively assumed to be equal to 2, as specified in 6.3 of EC8 [24]. This value is then reduced by 20% in order to account for the irregularity in elevation of both structures, as discussed in the
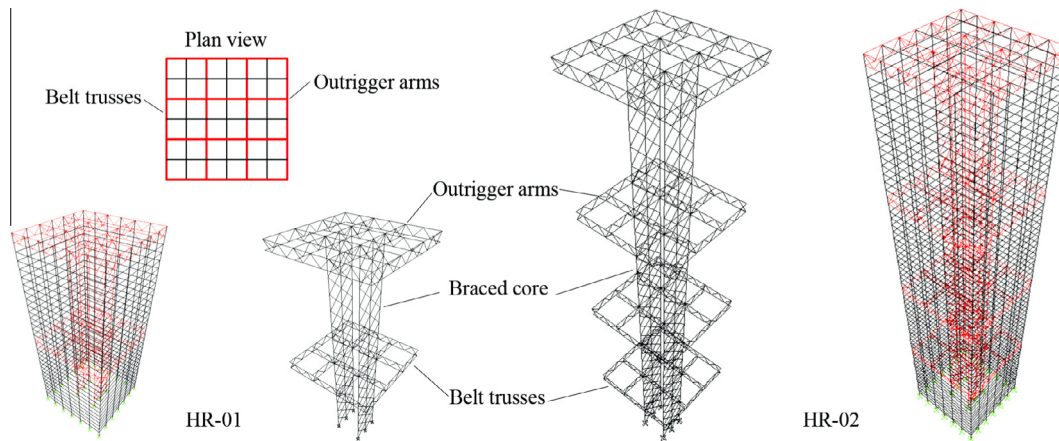
Fig. 1. Schematic of three-dimensional case-study buildings. Note: the bracing system of the core in transverse direction is hidden in this render view for easiness and readability of the primary LFRS studied by NLTHAs.
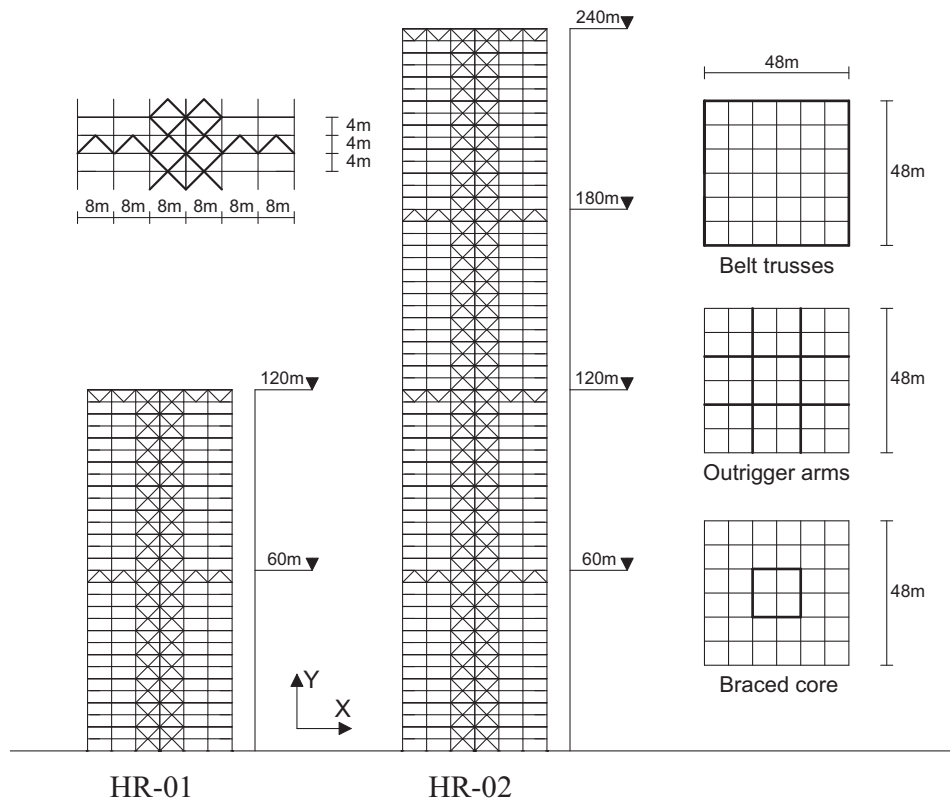

Fig. 2. Geometric characteristics and structural scheme of reference thirty- and sixty-storey planar frames.

following. Accordingly, the complete quadratic combination (CQC) scheme is chosen to conduct the RSA shown in Section 3.

The two structural layouts investigated are symmetrical in plan and their centre-to-centre square plan dimensions are 48×48 m at any floor, with a column spacing (S) of 8 m in both longitudinal and transverse directions. The columns have a constant inter-storey height (H) of 4 m, thus implying a total building height of 120 m and 240 m for HR-01 and HR-02, respectively. Dead and live loads are assumed to be 2 kN/m^2 and 4 kN/m^2, respectively. In addition, the self-weight of floor structure, internal partitions and external claddings are included in design process and FE analyses. The horizontal load due to wind pressure has been calculated according to ASCE-7 05 provisions [62], considering a basic wind speed equal to 37 m/s (84 mph). Assuming the buildings to be susceptible to overcrowding, vertical gravity loads in seismic combination conservatively consist of the dead loads and an allowance of 60% of live loads. The seismic masses at all floor levels of each planar frame prototype are chosen to be equal and to be applied on the beams, which are discretized using a one-to-six correspondence between structural members and model elements. To determine nodal masses and inherent point loads, the slabs are supposed to be unidirectional.

As mentioned, Figs. 1 and 2 show isometric, plan and elevation views of the super-tall buildings under study, presenting their structural scheme, while Table 1 summarizes their overall geometry and vertical design loads. In Table 2, member sizes and

Table 1
Case study mega-braced frame-core buildings: overall geometry and design loads.

	Overall MRF geometry				Design loads [kN/m²]	
	H [m]	# Floors [–]	S [m]	# Bays [–]	Dead	Live
HR-01	4	30	8	6 × 6	2	4
HR-02	4	60	8	6 × 6	2	4

mechanical properties adopted for beams, outriggers, columns and braces at different floor levels are collected. In detail, beams IPE 400 are used for the framing floor structure of both prototype buildings at any floor, while HD 400 × 634 and HD 400 × 1200 tapered profiles are assumed for the first five and twenty columns of HR-01 and HR-02, respectively. Similarly, braces HSS 300 × 20 and HSS 400 × 20 are provided in the first five and ten stories for HR-01 and HR-02, respectively. HD 400 × 314 profiles are selected to compose the outrigger members of both structures. Both brace and column sizes are designed to decrease along the height of the two super-tall case-study buildings, as presented in Table 2. Accordingly, q is scaled to 80%, thus resulting in a behaviour factor of 1.6. Considering this design target, inter-storey drift limits and second order effects are vital factors for such flexible earthquake-resistant structural systems. Code-compliant checks for serviceability limit state are performed in the initial analysis and design of the two case-study prototypes using RSA as reference analysis method. According to [63], steel grade S275 (i.e. f_{yk} = 275 N/mm²) and S450 (i.e. f_{yk} = 450 N/mm²) are chosen for beams and columns, respectively. In addition, the steel material used for both outriggers and braces is S700, with f_{yk} = 700 N/mm².

Fig. 3 shows an example of welded gusset-plate and bolted beam-to-column connection systems used to detail the joints of the two high-rise braced frame structures analyzed in this study. In particular, Fig. 3(a) sketches the geometry of the gusset plate used to connect the rectangular hollow section shape brace to the beam and column; fillet welds are provided between the web of the gusset plate and the rectangular HSS brace, while complete or full penetration welds (FPW) are designed to connect the edge of the gusset plate and the flanges of both beam and column. Table 3 collects the details of the gusset plates at different floor levels in HR-01 and HR-02 prototypes; their seismic design is conducted using the performance-based approach proposed by Nascimbene et al. [33], in compliance with the equations provided in the European rules [24] to estimate the resistance of each individual mode of failure. Furthermore, Fig. 3(b) presents the layout of a representative bolted beam-to-column connection used, in this case, to detail a partially-restrained joint at the first floor of HR-01 prototype. Three M20 × 80 – 10.9 bolts are used to bolt the shear tab to the web of the beam and two M20 × 80 – 10.9 bolts are provided between a 180 × 250 × 20 mm plate, welded by FPWs to the flange of the column, and the flange of the beam, in accordance with the prescriptions specified in [64]. Finally, the connection between the structure and its foundation is treated to be fixed in both design process and numerical simulations. Fundamental periods (T_1) equal to 2.73 s and 6.17 s are determined from eigenvalue analysis for HR-01 and HR-02 prototypes, respectively.

2.2. Modelling approach using fibre-based representations

In order to investigate the effectiveness of current European prescriptions when applied to super-tall buildings, these two

Table 2
Member sizes and mechanical properties in key structural components.

	30-storey frame – HR-01			60-storey frame – HR-02		
	Floor	Profile	Grade	Floor	Profile	Grade
Columns	1–5	HD 400 × 634	S450	1–20	HD 400 × 1200	S450
	6–10	HD 400 × 509	S450	21–30	HD 400 × 900	S450
	11–15	HD 400 × 421	S450	31–40	HD 400 × 634	S450
	16–20	HD 400 × 421	S450	41–50	HD 400 × 509	S450
	21–30	HD 400 × 237	S450	51–60	HD 400 × 314	S450
Beams	1–30	IPE400	S275	1–60	IPE400	S275
Outriggers	15/30	HD 400 × 314	S700	15/30/45/60	HD 400 × 314	S700
Braces	1–5	HSS 300 × 20	S700	1–10	HSS 400 × 20	S700
	6–15	HSS 250 × 16	S700	11–20	HSS 350 × 16	S700
	16–20	HSS 200 × 16	S700	21–30	HSS 300 × 16	S700
	21–30	HSS 200 × 16	S700	31–60	HSS 250 × 16	S700

Fig. 3. Details of (a) gusset-plate and (b) beam-to-column connections. Note: HR-01 – first floor.

Table 3
Sectional characteristics of gusset plates at different floor levels in HR-01 and HR-02 prototypes.

|	30-storey frame – HR-01		60-storey frame – HR-02	
	Floor	Width [mm] × thickness [mm]	Floor	Width [mm] × thickness [mm]
Gusset section	1–5	900 × 40	1–10	900 × 50
	6–15	700 × 30	11–20	900 × 40
	16–20	650 × 25	21–30	700 × 35
	21–30	650 × 25	31–60	700 × 30

design solutions are used to create accurate nonlinear models of the case-study structures which are then subject to NLTHAs, using a set of real accelerograms [25,26] scaled to an intensity level compatible with that assumed in design. The performance of the design method is then gauged by comparing design actions and deformations with those recorded in the NLTHAs. As specified in 4.3.3 of EC8 [24], four types of analysis can be used for seismic design and evaluation of structures:

1. Linear elastic static analysis.
2. Modal response spectrum analysis.
3. Nonlinear static analysis.
4. Nonlinear time history analysis.

Linear elastic static analysis based on the classical lateral force method for the definition of equivalent seismic loads is unfeasible for the two prototypes under investigation considering their irregularity in elevation (see 4.2.3.1(3)P of EC8 [24]). By contrast, multimodal RSA assuming a linear elastic structural model is recognized to be the reference method of analysis, as prescribed in 4.3.3.1(2)P of EC8 [24]. As an alternative to linear techniques, a nonlinear approach may also be used, since nonlinear static and dynamic analysis are explicitly permitted in the European seismic rules [24]. While the former presents intrinsic limitations [27–32], the latter is the most accurate simulation procedure as it can potentially incorporate many different interacting sources of material and geometric nonlinearity, directly taking into account the dynamic nature of loading. Being this analysis technique able to reproduce dynamic effects and propagation of damage throughout the structure in such a way that more closely reflects the physical nature of seismic excitation, NLTHAs will be assumed as reference in this study to compare the results of the simplest and most common analysis tool for design office use (i.e. RSA), in which plastic hinging mechanisms are included in a simplified manner.

Therefore, a series of NLTHAs have been performed to predict the seismic response of the two high-rise buildings under study, using the open source FE platform OpenSees [23] to construct fibre-based idealizations [60] able to account for geometric and material nonlinearities through classical corotational transformation and distributed plasticity approach [21]. In this computational framework, sectional stresses and strains are obtained through direct integration of the uniaxial material response of individual fibres. In detail, 3D inelastic force-based fibre elements with five integration points are used to model the structural frame members, assuming a bilinear stress–strain relationship with isotropic strain hardening to reproduce the permanent deformations exhibited by plastic materials during the loading–unloading history, thus simulating the spreading of inelasticity over the member length and cross section depth. One-to-one and one-to-six correspondence between structural members and model elements are considered for columns and beams, respectively. As previously mentioned, this discretization is prepared to permit the application of nodal seismic masses and corresponding gravity point loads in seismic combination.

Mechanical representations developed and validated in comparison with experimental tests and detailed numerical models [33–38,55–59] are integrated in OpenSees [23] to equivalently incorporate the complex response of bolted joints and bracing systems in the series of FE analyses carried out. In particular, Fig. 4 shows a schematic of the modelling approach used for brace and gusset-plate connections [33,34,58,59]. This inelastic 3D beam–column brace model, originally proposed by Uriz et al. [65], consists of two inelastic force-based beam–column elements, each of which having five integration points and a discretized fibre section. According to [65], all the fibre cross sections are subdivided into 20 layers across the depth and width. In order to capture the effects of gusset end restraint [33,34,58,59], the present paper takes advantage of an additional inelastic force-based beam–column element
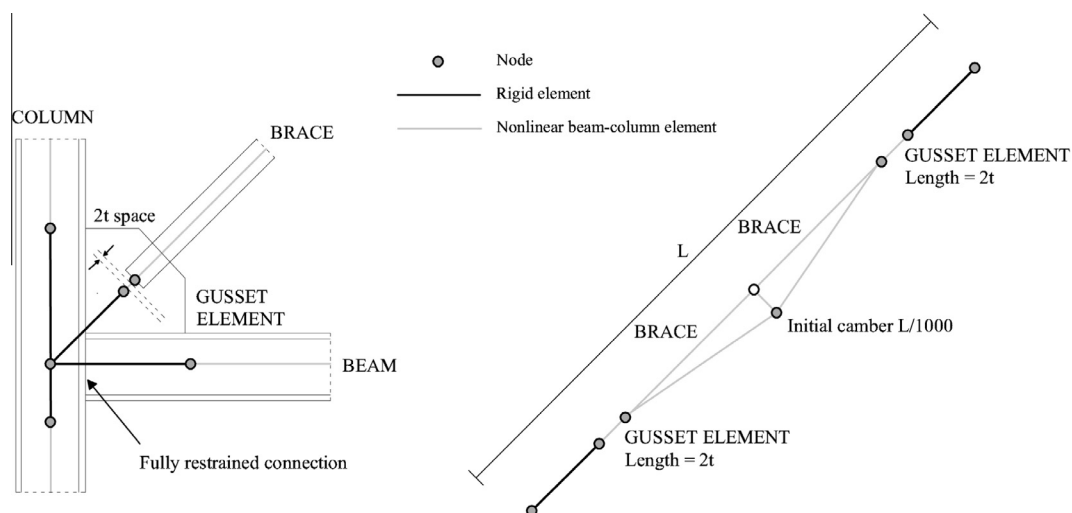
Fig. 4. Schematic of the modelling approach used for gusset-plate connections.

of length $2t$ – where t is the thickness of the gusset plate – at each end of the brace. As done in [33,34,58,59,65], the welds of gusset-plate connections are not explicitly modelled, while a set of rigid elements is included in FE modelling to represent the confined portions and geometry of beam, column and gusset plate. To account for potential buckling mechanisms in both braces and gusset plates, each braced frame is modelled in three-dimensions rather than in two-dimensions, thus permitting the brace to buckle in the out-of-plane direction of the frame. As suggested in [65], an initial out-of-plane imperfection equal to $L/1000$ – where L is the entire length of the brace – is imposed at its midspan, while the nodes of both beam and columns are restrained to deform in-plane only. The corotational theory is assumed to represent the moderate to large deformation effects and inelastic buckling mechanisms of the concentric braces, while small deformation theory is used to solve for local stresses and strains of the inelastic beam–column element. Therefore, this model is able to take into account geometric nonlinearities and inherent strength decays due to potential large displacements/rotations in critical portions of the braces. In addition, the axial force and bending moment interaction is reproduced by integrating the uniaxial hysteretic steel material model over their cross section. In particular, the Menegotto–Pinto material model is used for these members including isotropic hardening and Bauschinger effects [65].

The limitations and potentials of this approach were extensively examined and discussed by Wijesundara et al. [59], using test data from five different experimental programmes. While the inelastic brace model used herein was observed to predict with adequate accuracy loading stiffness, unloading stiffness and pinching behaviour when the brace is straightened out from the buckled configuration under tensile loading, this fibre-based idealization is unable to explicitly account for local (sectional) buckling effect in the post-buckling regime of the response. Once buckling occurs in the brace, inward bulging may develop in the portion of the cross section that is subjected to the highest compressive stresses due to combined axial and flexural response, thus resulting in a gradual ovalization of the cross section. Upon imposing higher axial deformations, the cross section may eventually flatten locally and a pronounced kink in the plastic hinge may possibly form, thus implying a reduction of compressive resistance. Even if the medium/low dissipative design target of the two case-study structures does not correspond to such a large deformation demand in the brace, the occurrence of post local buckling phenomenon may be predicted using high-definition solid or shell models [33,34]. Alternatively, more recent studies [66] have proven the effectiveness of fibre-based models when used to account for such a mechanism in a phenomenological sense. Peculiar stress–strain constitutive relationships with equivalent negative slopes were integrated in a classical fibre element formulation to represent the stiffness degradation and strength deterioration of hollow steel section members, each of which modelled using a single frame element.

Similarly, equivalent mechanical idealizations were assumed in past studies [35–38,55–57] to reproduce the cyclic behaviour of top-and-seat angle or T-stub bolted joints, thus including the significant earthquake-resistant potential of such partially-restrained connection systems in lumped or distributed inelasticity models. In light of this, a fibre-based representation [35–38] is prepared along the lines of classical component approaches [55–57], using a series of rigid links (i.e. elastic beam–column element object) to represent the geometry of the joint, in combination with nonlinear springs (i.e. zero-length element object) and fibre elements (i.e. force beam–column element object) introduced to simulate bolts and shear tab/top-and-bottom plates, respectively. A schematic of the assembly is shown in Fig. 5. As done for gusset-plate connections, FPWs are not explicitly included in FE
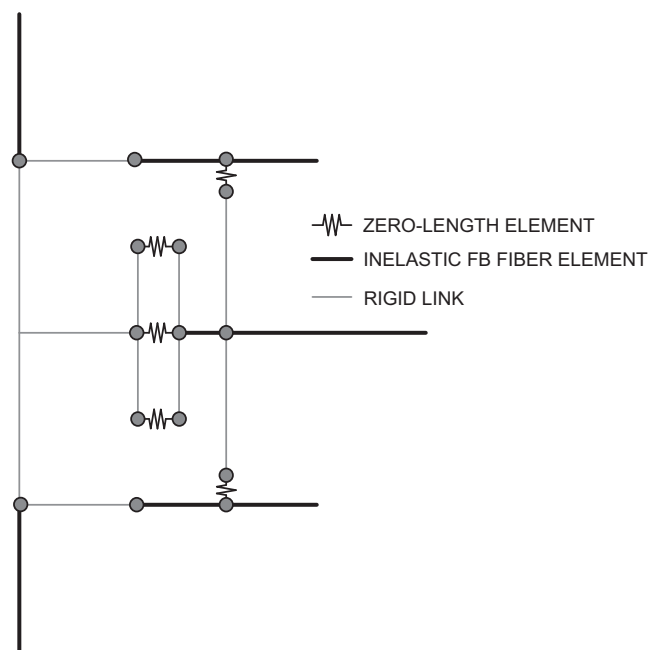

Fig. 5. Mechanical fibre-based idealization for bolted joint systems.

modelling, assuming them to behave as a full restraint-full strength component of the connection system. Conversely, the set of NLTHAs carried out accounts for material nonlinearities of plates and bolts. In particular, an elastic–plastic bilinear idealization with isotropic strain hardening is used for top-and-seat plates and shear tab. A bilinear cyclic constitutive law is assumed for nonlinear springs incorporating material properties and geometric characteristics of the bolts, in accordance with the component approach codified in Eurocode 3 (i.e. EC3) [67]. An additional gap element is added in parallel to simulate bolt–hole clearance [68]. The numerical approach proposed herein was validated in compliance with experimental tests on full-scale bolted connection systems [35–38] conducted as a part of the SAC Project [69].

The large displacement–small strain nonlinear dynamic analyses are conducted using a lumped mass matrix approach and the Krylov subspace algorithm to iteratively equilibrate loads, since it has a larger radius of convergence and requires fewer matrix factorizations than Newton–Raphson [70,21]. As done in [71,21], a tangent stiffness-proportional Rayleigh damping model calibrated on the first mode of vibration of the two mega-frame case-study structures is assumed to carry out the series of NLTHAs. Two modes of vibration (T_1 and T_2) with specified damping ratios (ξ_1 and ξ_2) are required to implement the conventional Rayleigh model, which is proportional to both mass and stiffness. In particular, Eq. (1) provides the expressions for mass matrix (α_M) and stiffness matrix (α_K) multipliers:

$$\alpha_M = 4\pi \frac{\xi_1 T_1 - \xi_2 T_2}{T_1^2 - T_2^2} \quad \text{and} \quad \alpha_K = \frac{T_1 T_2}{\pi} \frac{\xi_2 T_1 - \xi_1 T_2}{T_1^2 - T_2^2} \tag{1}$$

where T_1 and T_2 are the first and last modes of interest. Based on numerical and experimental comparisons examined by Grant and Priestley [71], the stiffness-proportional asymptotic branch of Rayleigh model is considered in this case to avoid an overdamped dynamic response. The stiffness-proportional matrix multiplying coefficient used for nonlinear dynamic analyses may be expressed as stated in Eq. (2):

$$\alpha_K = \frac{\xi T_1}{\pi} \tag{2}$$

where ξ is the damping ratio associated with the fundamental period of the structure. To overcome higher numerical instability, the tangent stiffness-proportional damping matrix is updated at every load increment rather than at every iteration. A classical displacement/rotation-based convergence criterion with a threshold set equal to 10^{-3} is adopted to perform the simulations, assuming an auto-update integration time-step of the order of one-tenth of the time sampling of the ground motions considered [25,26].

2.3. Seismic input: earthquake characteristics and basic criteria for selection

To carry out NLTHAs of structures, the dynamic excitation has to be specified in terms of accelerograms, and the influence of seismic input, as well as structural parameters and the level of inelasticity, is a crucial point for seismic response assessment [72,73]. While selecting, scaling and matching ground motions to obtain a compatible set of records play a key role in seismic analysis and earthquake-resistant design in order to determine reliable numerical estimates with an acceptable level of confidence, no unanimous consensus has been yet achieved on this subject.

According to EC8 [24], the time history representation of the ground motion is permitted using natural ground motions, artificial accelerograms and simulated records. When compared to real and artificial records, simulated accelerograms are usually adopted to a lesser extent in earthquake engineering practice, as they require a comprehensive knowledge of the seismotectonic setting of the area under study, as well as a large number of input parameters concerning earth crust rupture and travel path mechanisms. Furthermore, the ground motion characteristics of artificial accelerograms (e.g. frequency content, duration and phase correlation) are shown to be strongly dependent on the generation algorithm assumed and their prevailing features can differ from those of real time series. In contrast, ground motions recorded during seismic events are preferable because they possess a realistic low-frequency content, as recognized in EC8 [24].

In light of these considerations, a set of ten natural records scaled by Maley et al. [26] to obtain displacement spectrum compatibility according to EC8 requirements [24] is considered in this work to conduct the series of nonlinear dynamic analyses presented in the upcoming discussion. While further and more comprehensive information may be found in [25,26], the prevailing criteria for selecting and scaling this suite of accelerograms, originated from earthquakes ranging in magnitude from 6.2 to 7.6, are synthesized in the following. Table 4 summarizes the main ground motion characteristics of the ten (in lieu of seven) natural records considered in this research – ID, event, station, component, moment magnitude (M_W), closest distance from recording site to fault area (D), duration (t_{tot}) and shear wave velocity over the first 30 m (V_s) – and their scale factor (SF) for spectrum compatibility over a medium to large period range, which is in agreement with

the dynamic characteristics of the two case-study structures. The accelerograms were all selected from PEER NGA database and were all recorded on sites conforming to EC8 soil type C, as assumed in the initial design phase of the two mega-braced frame prototypes.

Several contributions [74–78] constitute the theoretical background for the scaling process carried out [26] with the aim to minimize the spectral misfit between geometric mean spectra and code-compliant design spectra over a medium to long period range. In particular, these studies [74–78] have addressed the question of selection and amplitude scaling of accelerograms for predicting the nonlinear seismic response of structures and have additionally explored the influence of magnitude–distance scenario, broadband spectral compatibility and long periods. Shome et al. [74], Iervolino and Cornell [75] and Hancock et al. [76] have remarked the importance to constrain the response spectral shape itself in a sufficiently large period range, showing that ground motion records can be multiplied by a constant scale factor with bounded values (i.e. SF < 10), without affecting substantially the stability of the FE estimates obtained by NLTHAs performed using these records. As presented in Table 4, the suite, obtained without introducing any frequency context adjustment using wavelet in order to match the target design spectra, takes advantage of SF less than 6 for all ground motions, except for record 02 (i.e. SF < 8). By contrast, this accelerogram provides a high contribution in terms of spectral accelerations.

Other research efforts [77,78], in which an exhaustive characterization of long period ground motions for seismic design of structures was proposed, have revealed that long period values can be expected in Italy and in other parts of the world [62], thus justifying the choice of a corner period (T_D) equal to 8 s (instead of 2 s) for the 5% damped target spectra. In fact, the acceleration and displacement response spectra shown in Fig. 6 correspond to EC8-compliant 5% damped type 1 spectra for a PGA of 0.40 g and soil type C, but with T_D equal to 8 s such that spectral displacement demands increase linearly up to this value of corner period [62,77,78]. To comply with European seismic rules [24], 5% damping was considered by Maley et al. [26]. As a result of this code-compliant input selection [24], ξ is assumed to be equal to 5% when performing both RSA and NLTHAs. Similar damping values were adopted in other numerical studies investigating the seismic response of high-rise buildings [1–3,9,13,14,25], even if lower ratios (i.e. 2–3%) may be conservatively used.

As depicted in Fig. 6, the average displacement and acceleration response spectra obtained from the suite of ground motions assumed in this work provide a satisfying match with the target design spectra over a medium (i.e. 1–4 s) to long (4–8 s) period range, as the coefficient of variation (COV) equals 0.22 and 0.12, respectively. The EC8-compliant displacement spectrum is well fitted with the average spectrum of the records in the interval 0–8 s and a similar consideration can be drawn for each single spectrum of the set. By contrast, a higher variation (i.e. COV = 0.42) can be

Table 4
Details of the natural ground motion records used in this research – adapted from Maley et al. [26].

| Record ID	PEER ID	Event	Station	Component	M_W [–]	D [km]	t_{tot} [s]	V_s [m/s]	SF [–]
01	1233	Chi-Chi, Taiwan	CHY082	E	7.62	36	90	194	2.1
02	1153	Kocaeli	KOERI Botas	090	7.51	127	102	275	7.9
03	851	Landers	CDMG 14368 Downey – Co	000	7.28	157	70	272	4.0
04	1810	Hector	Mecca – CVWD Yard	090	7.13	92	60	345	2.9
05	1629	St Elias, Alaska	USGS 2728 Yakutat	279	7.54	80	83	275	1.5
06	777	Loma Prieta	USGS 1028 Hollister City Hall	090	6.93	28	39	199	1.8
07	1043	Northridge-01	Neenach – Sacatara Ck	090	6.69	52	48	309	5.8
08	728	Superstition Hills-02	Westmorland Fire Sta	180	6.54	13	40	194	2.3
09	172	Imperial Valley-06	El Centro Array #1	140	6.53	22	39	237	5.1
10	2615	Chi-Chi, Taiwan-03	TCU061	N	6.20	40	107	273	5.6
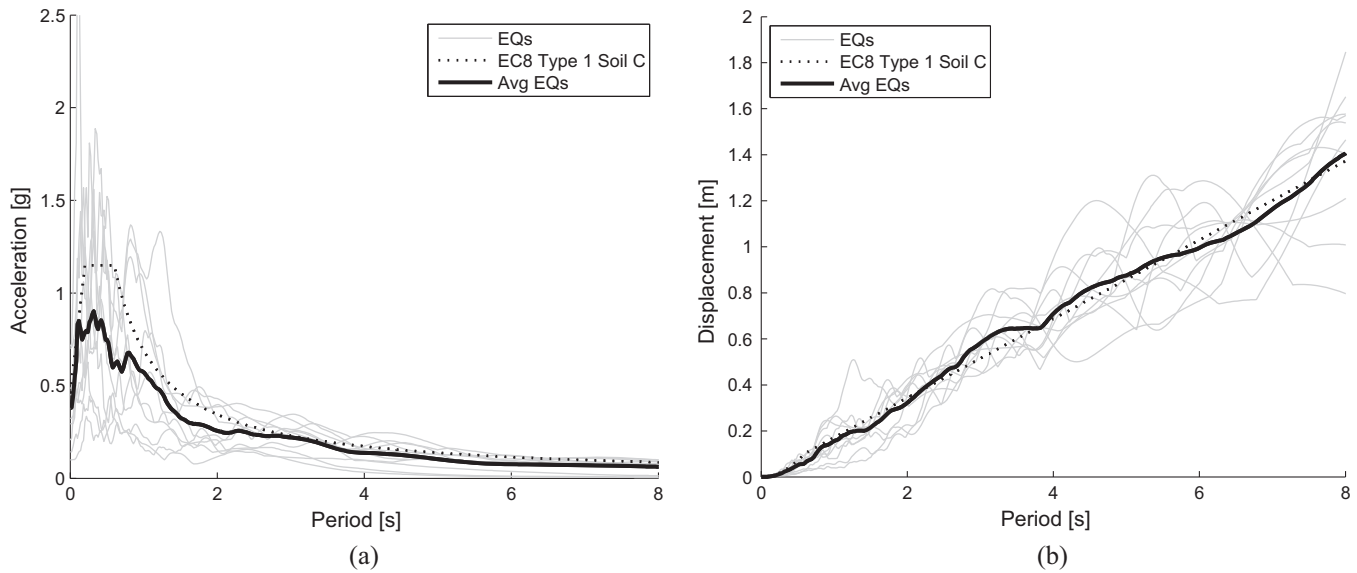
Fig. 6. Seismic input: (a) acceleration and (b) displacement elastic response spectra [25,26].

observed in the short period range (i.e. 0–1 s), as a consequence of spectral accelerations lower than those presented by the target design spectrum.

3. Results and discussion

The main results obtained from the series of numerical analyses carried out will be summarized in the following. In particular, the responses of the two high-rise mega-frame structures under study will be compared and used to describe and discuss the global and local behaviour of their lateral-force resisting systems, when subjected to severe earthquake-induced demands. A general overview of their prevailing characteristics is given here, and specific aspects are referenced when needed to explain key points. Particular care is paid to the response of hollow section shape braces and gusset-plate connections, showing their influence on the global structural performance of these two super-tall mega-braced frame-core building prototypes.

Furthermore, a paradigm will be then developed to relate the seismic behaviour of the same structural prototype using different types of analysis (i.e. linear dynamic response spectrum analysis and nonlinear dynamic response history analysis). Codes [24,62,79–81] and research studies [72,73,82,83] have extensively examined the viability of this type of comparison and several proposals have been made over the last decades to predict nonlinear deformations and forces through linear methods of analysis. Instead of performing a nonlinear analysis, inelastic effects may be indeed accounted indirectly in linear analysis methods by means of specific response modification coefficients and deflection amplification factors that are dependent on the structural system and ductility class/level. According to Uang [82], the force reduction factor (FRF) and the deflection amplification factor (DAF) can be expressed as reported in Eqs. (3) and (4), respectively:

$$FRF = R_\mu \Omega \tag{3}$$

$$DAF = \mu_s \Omega \tag{4}$$

where μ_s is the system ductility factor, R_μ is the ductility reduction factor and Ω is the structural overstrength factor. Following the research of Uang and Maarouf [83], the ratio between DAF and

FRF equals the ratio between inelastic drift (Δ_{max}) and elastic drift (Δ_e), as stated in Eq. (5):

$$\frac{DAF}{FRF} = \frac{\mu_s \Omega}{R_\mu \Omega} = \frac{\mu_s}{R_\mu} = \frac{\Delta_{max}}{\Delta_e} \tag{5}$$

It is recognized that use of values of DAF less than FRF underestimates deflections [72,73,82,83]. In particular, Uang and Maarouf [83] investigated the response of a two-storey eccentrically braced frame and a thirteen-storey steel moment frame, quantifying the variation of their maximum storey drift as a function of the earthquake intensity. Their estimates revealed that the DAF-to-FRF ratio increases with the system ductility reduction factor. Within the practical range of interest of their research (i.e. R_μ in the range 1–5), this parameter was proven to vary from 1.0 to 1.5. More in detail, ratios of up to 10% higher than unity were observed for moderate structural ductility levels (i.e. R_μ in the range 1–2.5) that are in closer agreement with those assumed in this study.

While US recommendations [62,79] propose two different dedicated factors for force and deflections, EC8 [24] uses the equal displacement rule in most cases, implicitly assuming DAF and FRF to be equal to the behaviour factor (q). This EC8-compliant procedure was used to obtain the set of RSA-based results presented in the upcoming discussion. In addition, it can be noted that the deflection amplification factors proposed in US provisions are in general either equal to or lower than the corresponding force reduction factor, depending on the structural system and its level of inelasticity [72,73]. As a result, the US provisions are less conservative when compared to EC8, since the latter approach considers the DAF-to-FRF ratio as unity.

3.1. Global performance of mega-frame systems

The global responses of the two super-tall buildings studied are provided in Figs. 7 and 8, in terms of inter-storey drift and acceleration peak profiles from RSA and NLTHAs. In particular, Figs. 7 and 8 present the peak values recorded for each accelerogram, together with their average, for the thirty- and sixty-storey mega-frame prototypes, respectively. In addition, the peak displacements obtained at each floor are collected in Fig. 9 for both structures.

As shown in Figs. 7(a) and 8(a), the average storey drift demands are much higher than the design storey drift capacities from RSA, particularly for the sixty-storey building (see Fig. 8(a)),
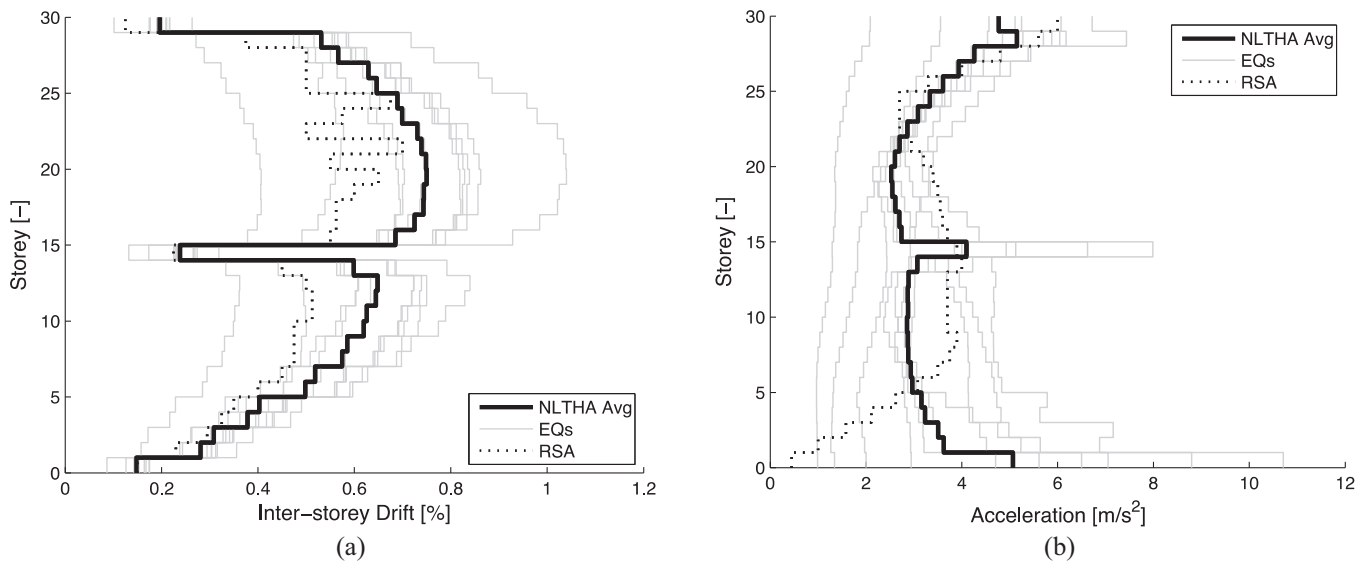
Fig. 7. Prototype HR-01: (a) inter-storey drift and (b) acceleration peak profiles from NLTHAs and RSA.
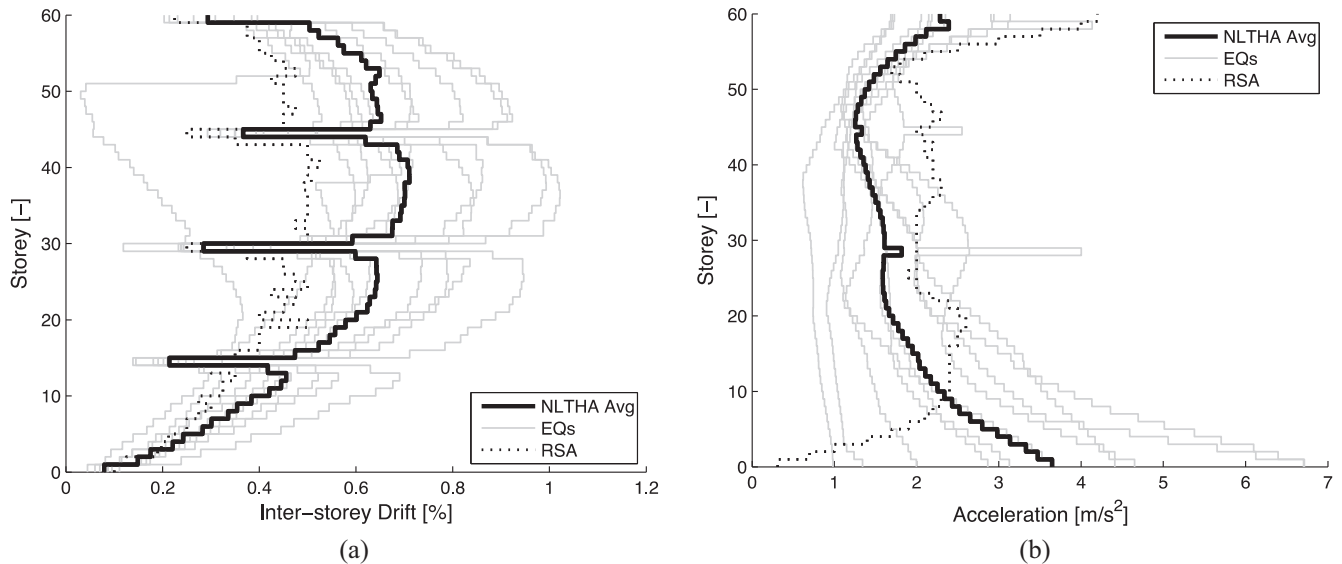

Fig. 8. Prototype HR-02: (a) inter-storey drift and (b) acceleration peak profiles from NLTHAs and RSA.

while an opposite trend is observed in terms of horizontal floor accelerations (see Figs. 7(b) and 8(b)). By contrast, the average horizontal displacement profile from NLTHAs appears to be relatively well captured by RSA, particularly for HR-01 prototype. For the thirty-storey case-study structure the displaced shape is well predicted over the bottom half of the building but over the upper stories RSA tends to be unconservative. As the building height increases, the discrepancy between RSA and the average of NLTHAs increases significantly, because of the nonlinear response of the structure that is characterized by a more pronounced higher modes contribution which in turn forces a different distribution of storey ductility demand to occur over the building height. In light of this, inter-storey drift and acceleration peak profiles from NLTHAs and RSA are also visibly different in shape, particularly for HR-02 due to more prominent effects of the higher modes in the tallest of the two prototypes (see Figs. 7(a) and 8(a)).

Peak roof displacements of up to 0.77 m and 1.83 m are observed for HR-01 and HR-02, in the case of the most severe

record, while values of about 0.61 m and 1.17 m are computed in average, thus showing peaks 20% and 36% lower for HR-01 and HR-02, respectively. As expected, the influence of higher modes is more visible in terms of drifts than displacements. Furthermore, the scatter of predictions from nonlinear dynamic analyses is higher in the latter case-study structure (see Fig. 9), due to a slightly higher scatter in the seismic input for a longer period (see Fig. 6). RSA deviates from the average of the ten NLTHAs performed at approximately mid-height of the structures, reaching a discrepancy of about 10% and 20% at the top storey of the thirty- and sixty-storey buildings, respectively. A fairly cantilevered displacement shape, with pronounced discontinuities in correspondence to the outriggers, is predicted for both structures (see Fig. 9) and this trend is even more visible in terms of inter-storey drifts and accelerations, as evidenced in Figs. 7 and 8. In detail, peak inter-storey drifts of approximately 0.75% and 1.00% are shown to occur at roughly two-thirds of the total structural height for both HR-01 and HR-02 in average and in case of the most severe
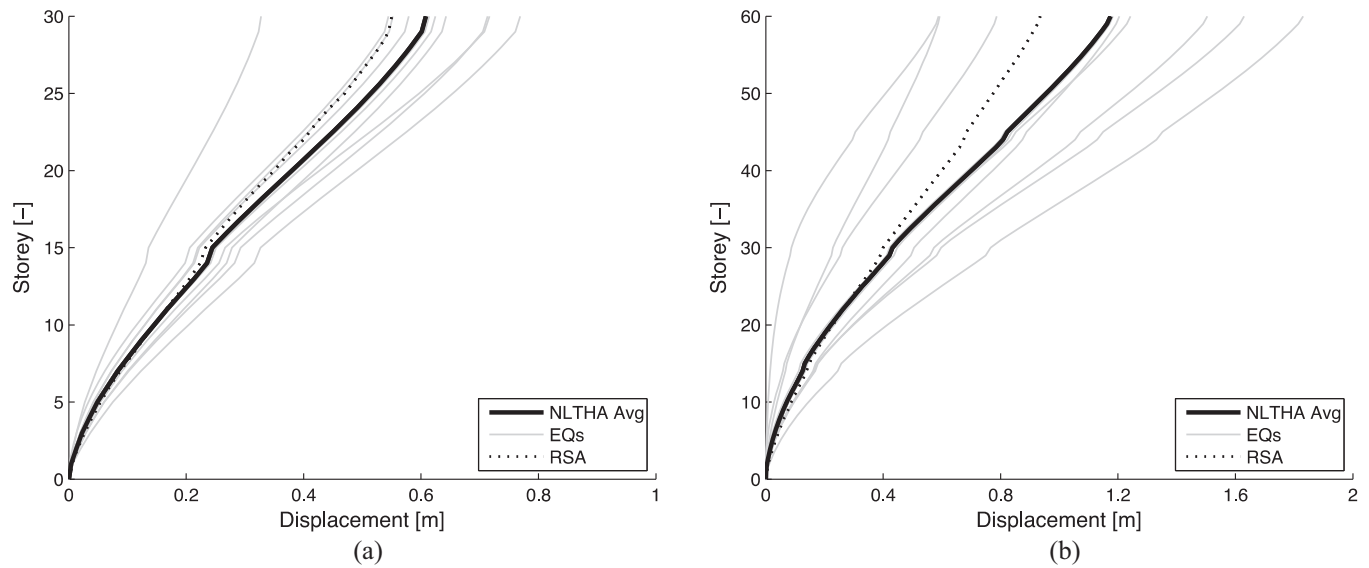
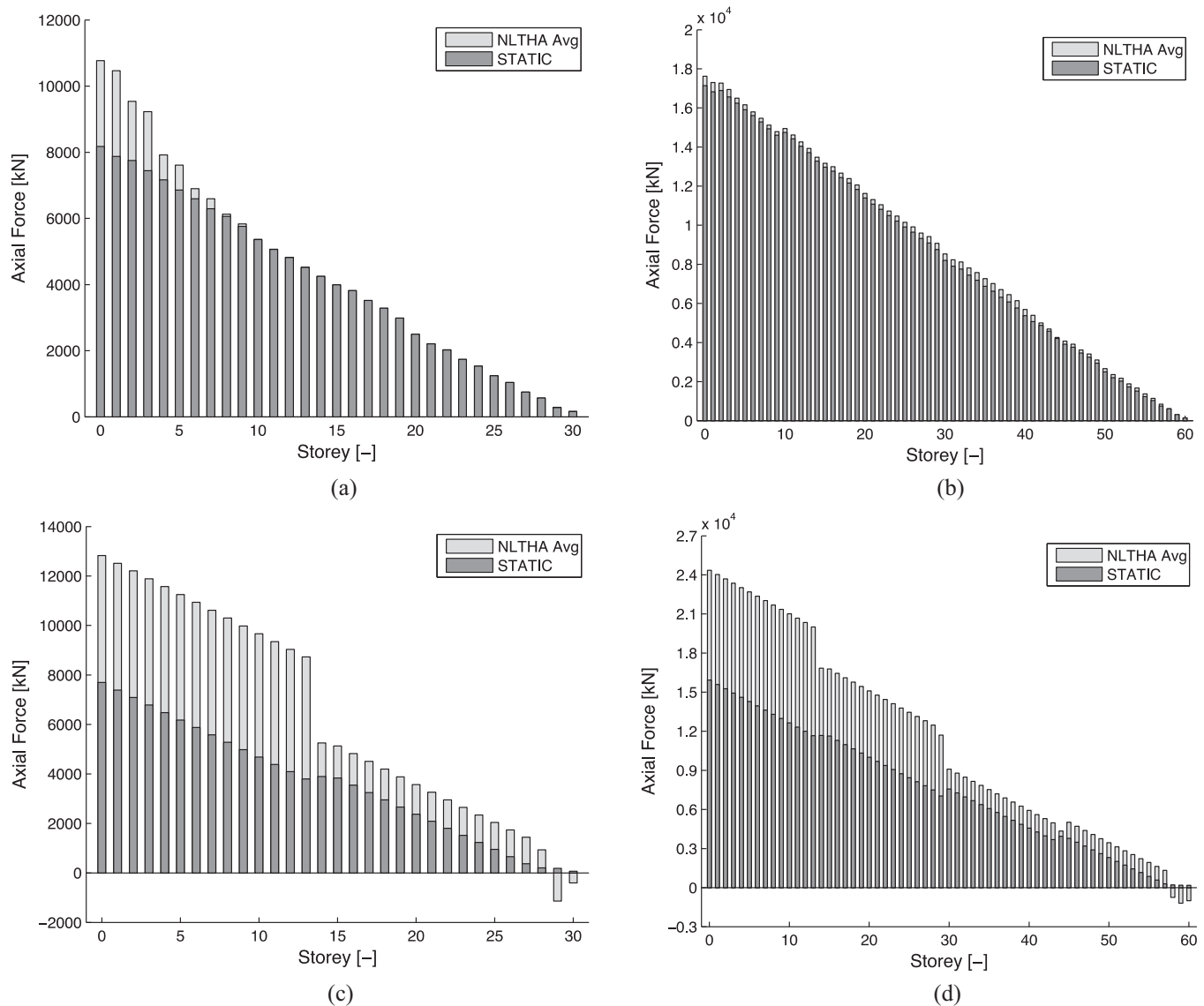**Fig. 9.** Peak lateral displacement profiles for (a) HR-01 and (b) HR-02 prototypes.

Fig. 10. Static vs. seismic demand: axial force peak profiles in the central column of (a) HR-01 and (b) HR-02 and in the leftmost column of (c) HR-01 and (d) HR-02, respectively.
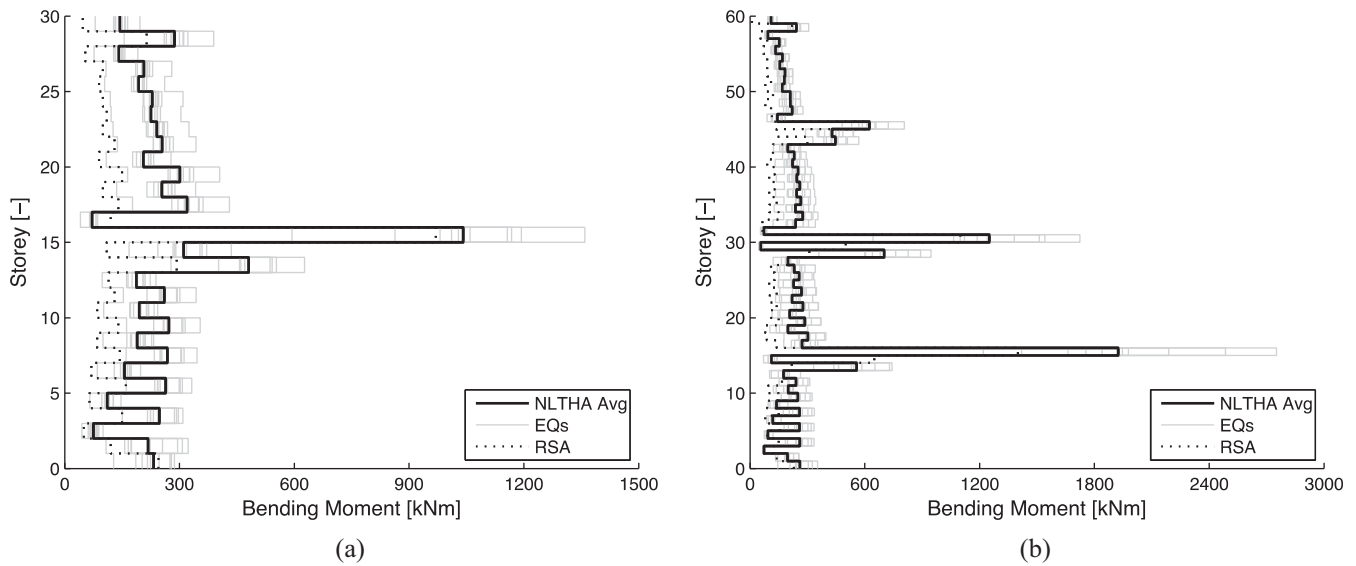
Fig. 11. Bending moment peak profiles in the leftmost column of (a) HR-01 and (b) HR-02, respectively.
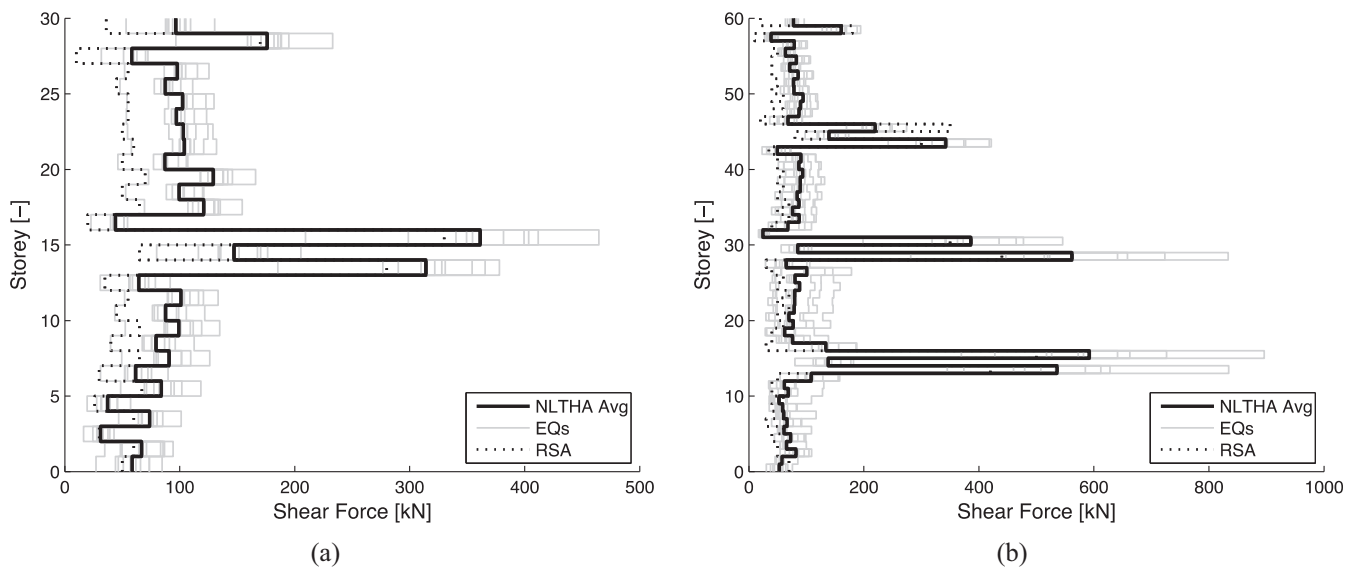

Fig. 12. Shear force peak profiles in the leftmost column of (a) HR-01 and (b) HR-02, respectively.

record, respectively. Therefore, the stiffening effect provided by the outriggers is proven to be significant for both building prototypes, as evidenced by a pronounced reduction in terms of inter-storey drifts experienced during nonlinear dynamic simulations. Peaks more than halved, in comparison with those recorded at the floor above and below the outrigger, are predicted for both structures. By contrast, these members caused a significant increase in acceleration and storey shear force demand in correspondence to them, as discussed later on.

This trend is particularly evident for the stiffest of the two super-tall mega-braced frame-core buildings – HR-01 – which has a fundamental period more than halved in comparison with that determined for HR-02 (i.e. 2.73 s vs. 6.17 s). The average peaks in terms of floor acceleration are approximately 0.53 g and 0.37 g in HR-01 and HR-02 prototypes, respectively. Maxima of up to 1.09 g and 0.68 g are experienced by the two structures during

NLTHAs, if the most severe ground motion is assumed as reference. Finally, the higher mode contribution is confirmed to be pronounced particularly in the upper stories of the tallest mega-braced frame building, as a consequence of its higher flexibility. Hence, the series of nonlinear dynamic simulations conducted have confirmed the significant potential of braces and outriggers/belt trusses when included in the LFRS of modern high-rise buildings, also showing that, if accurately designed and detailed, these structural systems provide an optimum combination of overall stiffness and strength, being these members able to induce a good balance between inter-storey drift and acceleration demands. Nonetheless, the structural response obtained for both case-study prototypes reaffirm the importance of maintaining uniform excess-strength ratios [24] over the building height, when sizing these structural components for lateral earthquake resistance, in order to ensure globally distributed dissipation and to
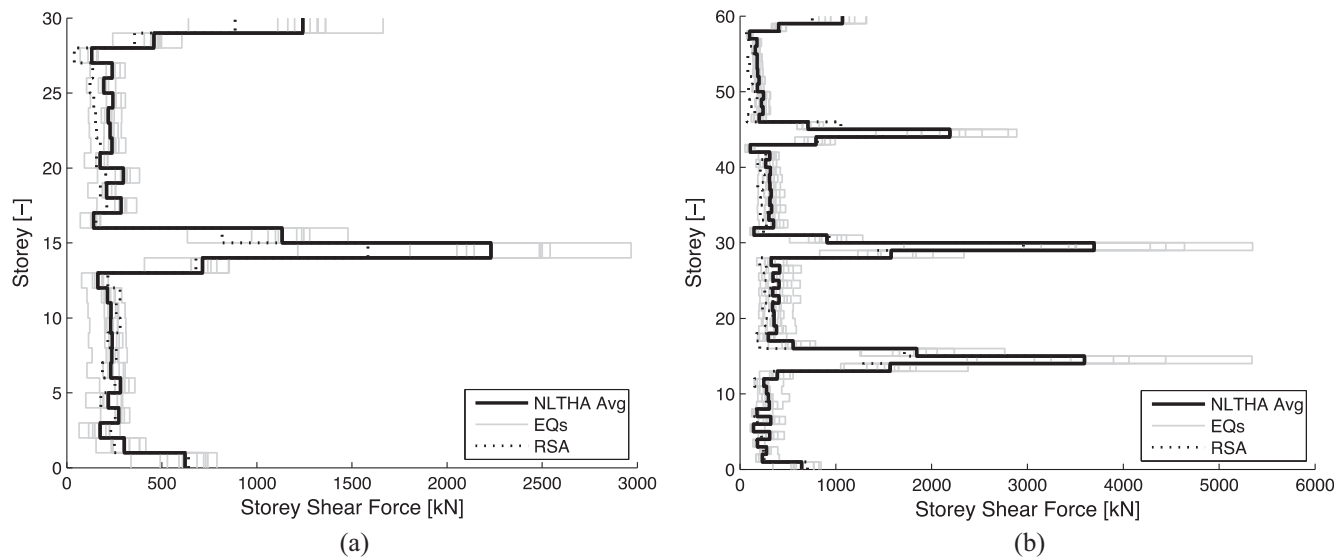
Fig. 13. Storey shear force peak profiles for (a) HR-01 and (b) HR-02 prototypes.
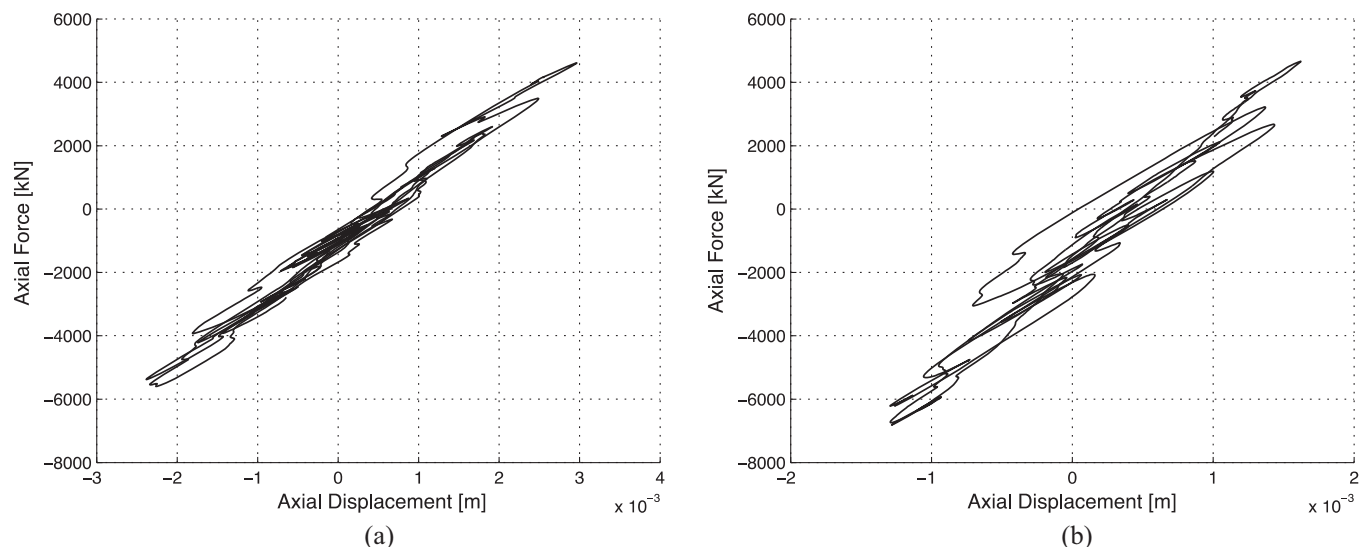

Fig. 14. Hysteretic behaviour of a critical brace at the first floor for (a) HR-01 and (b) HR-02.

prevent too high storey shear forces and accelerations from concentrating in a single storey where large differences in this parameter occur from one level to another.

3.2. Local response of key structural components

Once the global behaviour of the two high-rise structures were quantified, the local performance of their key structural components, such as columns, braces and outriggers, will be discussed in detail. In particular, axial load, bending moment and shear force peak profiles in different columns, as well as the hysteretic response of critical braces in terms of axial force–displacement curves will be shown to quantify their influence on overall structural response. In addition, the peak profiles of the earthquake-induced axial overloads (i.e. seismic vs. static axial force demand) will be computed for two reference columns of both structures.

To highlight the effects caused by the in-plane rotation of the outriggers at different floor levels, Fig. 10 collects the set of earthquake-induced compressive loads experienced by the

leftmost and the central columns of HR-01 and HR-02 in comparison with those produced by vertical loads in static conditions (i.e. dead and live loads in seismic combination). As expected, the central columns of both case-study mega-braced frame buildings are shown to remain almost unaffected by the dynamic excitation imposed at their base, since negligibly small extra-loads are observed, particularly for HR-02 prototype. By contrast, the contribution to lateral resistance ensured by the outriggers causes significant compressive overloads to be transferred to the lateral columns. In detail, an approximately 40% and 30% increase is computed at the base of HR-01 and HR-02, respectively; as the height of the structure increases, this overturning effect tends to decrease, showing a roughly linear piecewise decaying slope with the structure height. Pronounced discontinuities are again predicted in correspondence to the outriggers.

In light of the aforementioned considerations, only the numerical results recorded for the leftmost column of both mega-braced frame-core structures will be presented hereafter. In particular, the bending moment and shear force peak profiles predicted by
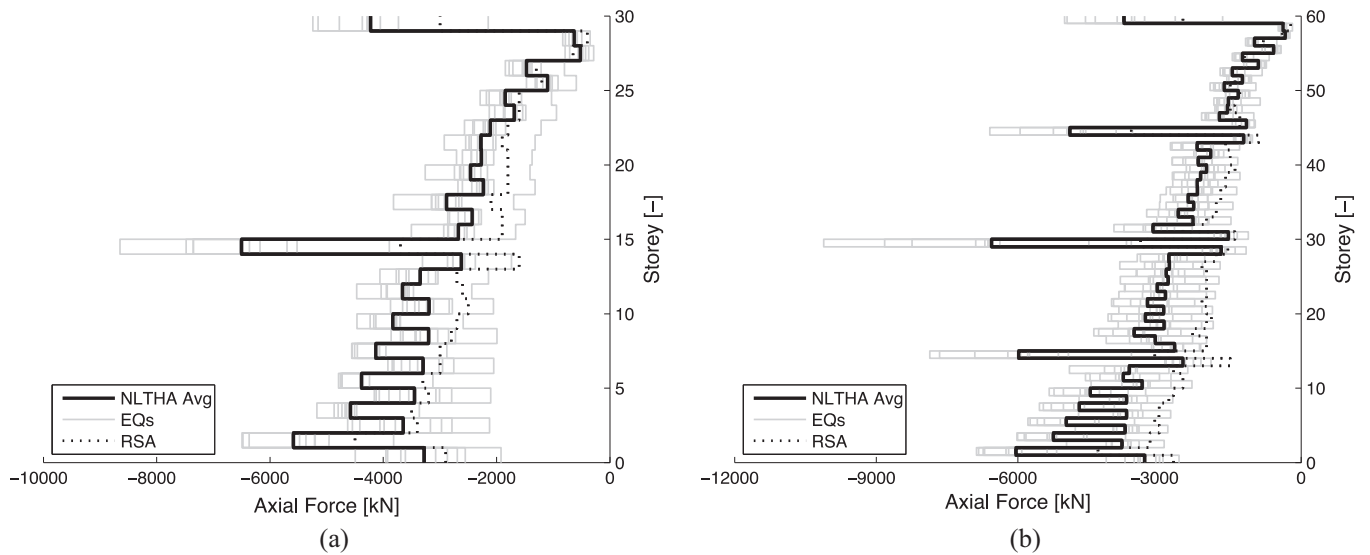
Fig. 15. Compressive force peak profiles in a critical brace of the core for (a) HR-01 and (b) HR-02, respectively.
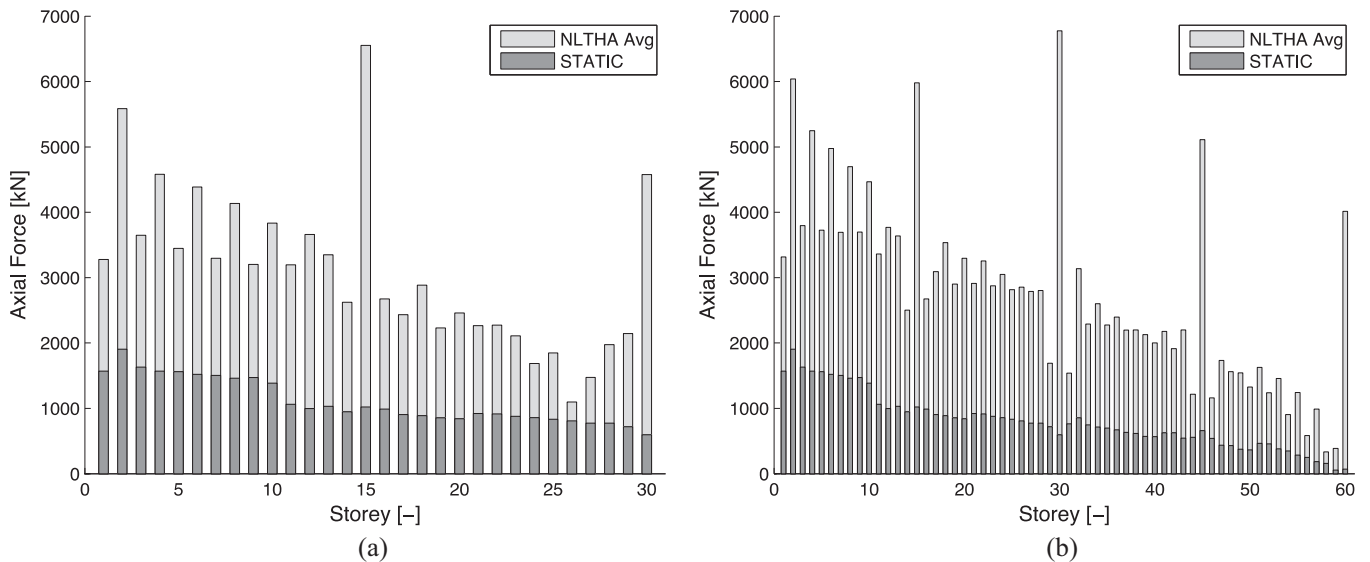

Fig. 16. Static vs. seismic axial load peak profile in a critical brace of (a) HR-01 and (b) HR-02, respectively.

NLTHAs and RSA are provided in Figs. 11 and 12 for HR-01 and HR-02 prototypes. High concentrations are again determined in correspondence to the floor levels where the outriggers are placed, as a consequence of those highlighted in terms of storey acceleration (see Figs. 7(b) and 8(b)). A similar consideration can be drawn in terms of storey shear force peaks for both case-study buildings (see Fig. 13). As previously discussed in terms of global structural behaviour (i.e. storey drifts and accelerations), RSA tends to significantly underestimate bending moment and shear force demands from the average of NLTHAs; in some cases, values more than halved are determined for both case-study structures (see Figs. 11 and 12).

An example of the axial force–displacement capacity curves predicted in a brace at the first floor is presented in Fig. 14, aiming to characterize the hysteretic behaviour of such a critical member. A nearly pseudoelastic cyclic response governed by strength rather than ductility can be observed for both HR-01 and HR-02 structures. The narrow hysteresis loops determined are shown to be too unstable to develop a well-established dissipative mechanism. This moderate plastic behaviour is in close agreement with the medium/low dissipative behaviour assumed as design target for both structures. As a result, these members visibly contribute for stiffening and strengthening of the overall building prototypes without adding significant energy dissipation at this structural performance level. Compressive peak forces of up to 5000 kN and 7000 kN are obtained, in this case, for the thirty- and sixty-storey case-study buildings, respectively. As highlighted in Fig. 15, where the compressive force peak profiles constructed for HR-01 and HR-02 are provided, a similar demand is predicted in average in the upper stories where the outriggers are placed. RSA is confirmed to underestimate the average of NLTHAs, particularly in the bottom and intermediate floor levels. This trend is evident for both case-study structures, even if it is more pronounced in the tallest of the two mega-braced frame-core prototypes (i.e. HR-02). Nonetheless, a peak discrepancy of about 40% is observed for both structures, if RSA and the average of NLTHAs are compared.
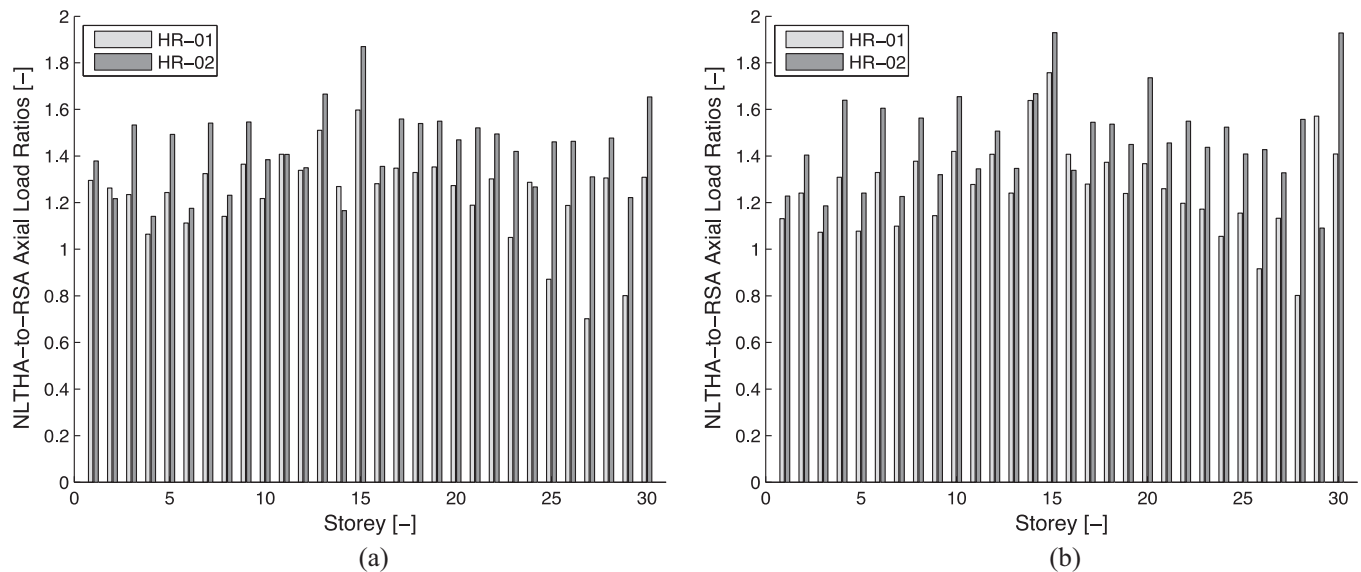
Fig. 17. NLTHA-to-RSA axial load ratios in the (a) leftmost and (b) rightmost brace of the core.
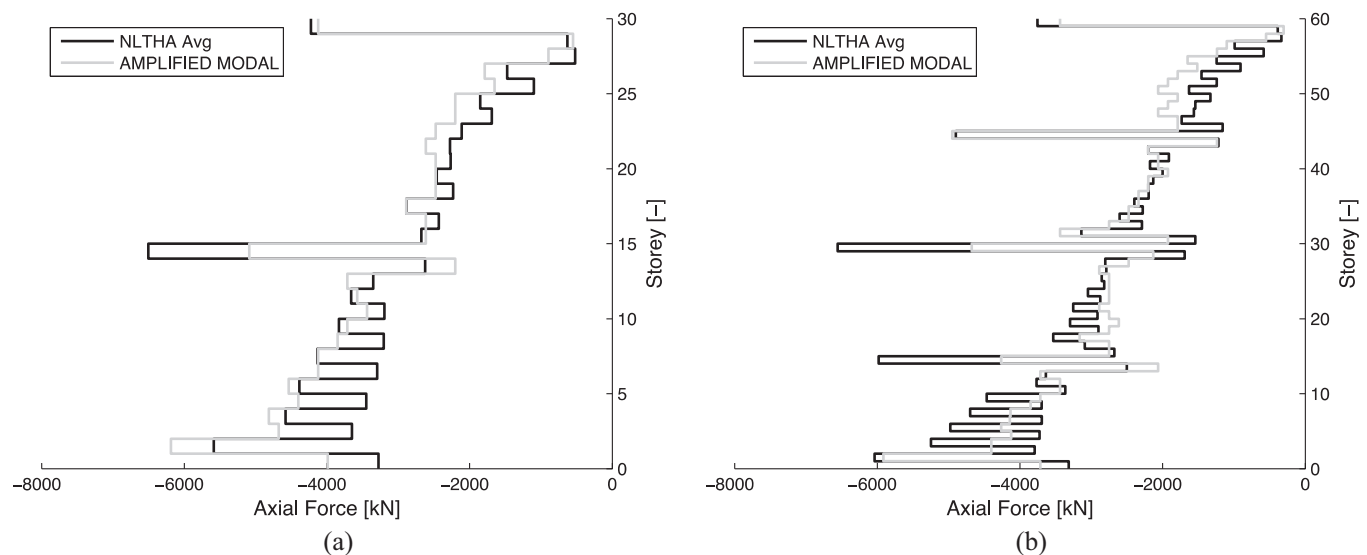

Fig. 18. NLTHAs vs. EC8-based demand: axial load peak profiles in a critical brace of (a) HR01 and (b) HR-02.

In Fig. 16, a comparison is provided between the compressive peak loads determined under seismic excitation and static condition, in the most critical brace of both high-rise frame-core buildings. Dynamic effects much more pronounced than those evidenced in the columns can be observed for this type of member. Furthermore, Fig. 17 collects the sets of NLTHA-to-RSA axial force ratios computed in leftmost and rightmost braces of the building core in order to quantify the discrepancy predicted in the critical components of the two reference buildings, using analysis methods with different levels of sophistication. The inaccuracy and unsafety level of RSA results in maxima at floor levels where the outriggers were placed, as they cause an abrupt change in the lateral stiffness of adjacent stories. In particular, the NLTHA-to-RSA axial load ratios reveal peaks roughly close to 2 at mid-height of both structures (i.e. 15th and 30th stories of HR-01 and HR-02, respectively). This large mismatch arises from the fact that multimodal RSA is characterized by intrinsic deficiencies and limitations for accurate predictions of both dynamic effects and plastic hinging mechanisms of a structure. In detail, this analysis procedure

superimposes and combines the contribution of different modes of vibration with their participating modal mass ratios and accounts for the level of inelasticity of a building by means of a unique behaviour factor for the overall structural system, assuming the contribution of each mode of vibration to be the same for dissipation purposes. Therefore, this simulation technique is unable to predict the concentrations of dynamic forces in critical portions of the structure which in turn cause the building to move further in the nonlinear regime of its response. As a result, this approach cannot reproduce the propagation and evolving distribution of damage/plastic hinging mechanisms in the structure at a local/element level, even in the case that a low/medium dissipative behaviour is assumed as performance level.

Being the mismatch between RSA and the average of NLTHAs in the braces higher than that observed in other structural elements, particular care has to be paid to the earthquake-induced demand assumed to design the related connection systems. In particular, EC8 provisions [24] recommend the following equation to be used for this purpose:
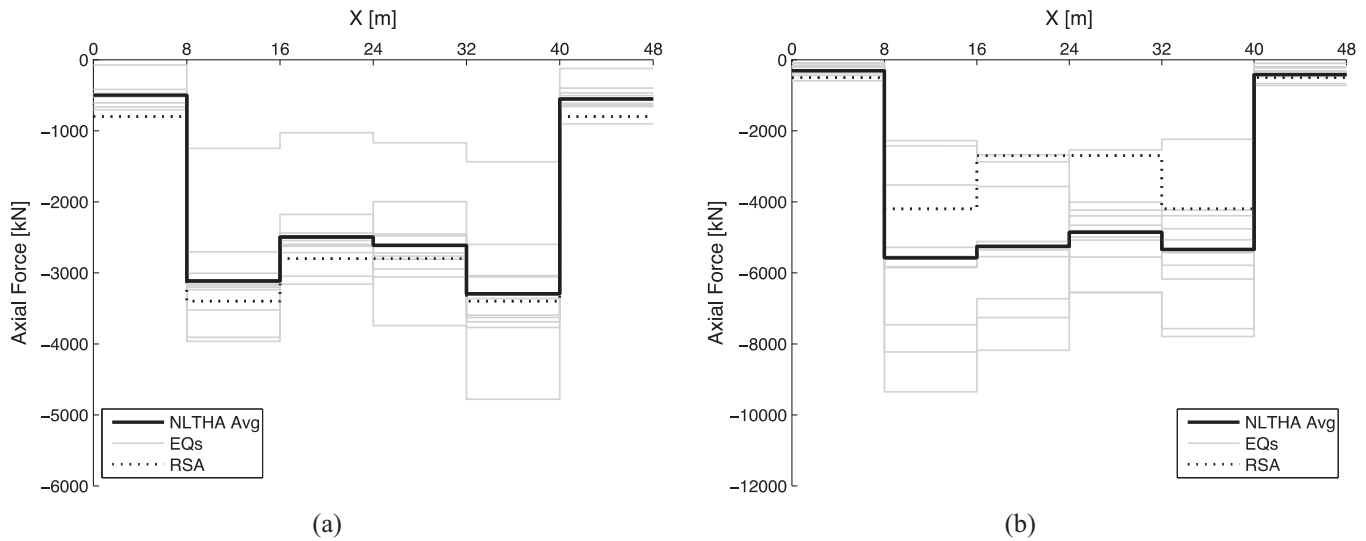
Fig. 19. Axial force peaks in the outriggers at the 30th storey in (a) HR-01 and (b) HR-02, respectively.

$$R_d = 1.1\gamma_{ov}R_{fy} \qquad (6)$$

where R_d is the axial resistance of the connection, γ_{ov} is the material overstrength factor and R_{fy} is the plastic resistance of the connected dissipative member. In Fig. 18, this EC8-based methodology is therefore compared, in terms of axial load peak profiles, with the average demand determined by NLTHAs. Even if the average forces obtained from them are found to align well with design values in the upper stories of both case-study mega-braced prototypes, the former approach is shown to provide unconservative estimates over the bottom half of the building, particularly in correspondence to the outrigger belts, thus confirming these elements to be the actual critical areas for structural system of this type. The EC8-compliant overstrength criterion expressed in Eq. (6) is neither accurate nor conservative in these vital portions of the two buildings under investigation (e.g. 15th and 30th stories of HR-01 and HR-02 structures), as the corrective coefficients proposed are unable to absorb and solve the inaccuracy of multimodal RSA, which directly causes the mismatch with nonlinear dynamic predictions. Hence, Fig. 19 presents a comparison between the peak axial loads predicted by RSA and NLTHAs in the outriggers placed at the 30th storey of the two reference structures. Even though a negligibly small difference can be observed between the two analysis techniques for the thirty-storey case-study building, a larger discrepancy is determined in the outriggers placed at mid-height of HR-02 prototype. This issue should be adequately dealt with in the earthquake-resistant design of such high-rise structures, limiting the excess-strength ratio over the building height and using accurate simulation approaches for seismic response assessment.

4. Conclusions

This paper focuses on the seismic behaviour of super-tall mega-braced structures, including outriggers and belt trusses in their LFRS, and presents the details of a modelling procedure to be implemented in an open source FE code for simulating their large displacement inelastic dynamic response. Thirty- and sixty-storey planar prototype frames, extracted from three-dimensional reference buildings, were designed according to European prescriptions and then fibre-based FE models were developed for seismic response assessment of these two case-study structures analyzed to examine both global and local performance of structural system and key components. Inelastic

force-based fibre elements were used to represent the frame members and mechanical fibre-based idealizations were prepared to reproduce the cyclic behaviour of bolted beam–column joints and welded gusset-plate connections. NLTHAs were performed in comparison with RSA, using a suite of ten natural displacement spectrum compatible records as a severe seismic input. The prevailing observations and conclusions drawn from the numerical simulations carried out can be summarized as follows:

- A pseudoelastic response governed by strength rather than ductility was obtained for both high-rise structures, thus showing bracing systems and outrigger belts to be effective in limiting inter-storey drifts and second order effects. In particular, peak inter-storey drifts of up to 0.75% and 1.00% were predicted to occur at two-thirds of the total structure height, whether the average of NLTHAs and the most severe ground motion of the suite are considered, respectively.
- Visible and abrupt changes/discontinuities in displacement, inter-storey drift and floor acceleration peak profiles were recorded and shown in correspondence to the outrigger arms, as a consequence of the significant stiffening effect provided by them. This in turn caused a large increase in bending moment and shear force demands in columns, HSS braces and welded gusset-plate connections, thus confirming the importance of limiting the excess-strength ratio over the building height. To mitigate force concentration due to sudden change in lateral stiffness, the stories above and below the outriggers may be stiffened/strengthened and the regularity of the structure in elevation may be enforced through increasingly optimized iterative design procedures. As a result, these can prevent a reduction of the behaviour factor, which is desirable especially when the performance of the building moves to a high dissipative design target in high ductility class (DCH).
- The effects caused by the in-plane rotation of the outriggers were proven to be negligibly small in the central column of both case-study prototypes, while high extra-loads of up to 40% were transferred to the lateral columns. In particular, the compressive force peak profiles were characterized by an approximately linear piecewise decaying slope with the structure height, presenting pronounced discontinuities in correspondence to the outrigger belts, which are confirmed to be the critical areas for super-tall structural systems of this type.

- RSA tends to largely underestimate the average of NLTHAs and in some cases values more than halved were determined, in terms of local demands on key structural components; a similar consideration can be drawn for peak displacements and inter-storey drifts. Therefore, the use of NLTHAs as a post-design check is reaffirmed to be a crucial aspect for these high-rise mega-braced frame-core buildings, the response of which is significantly affected by higher mode effects, particularly at the top stories.

- Sensitivity to the structure height was investigated by comparing the responses of the two reference structures under study, thus showing current European seismic rules to impose a similar performance for both HR-01 and HR-02 prototypes, in terms of global and local behaviour. When accurately designed and detailed in light of capacity design principles and performance-based design concepts, bracing systems and outrigger belts were demonstrated to provide an optimum combination of stiffness and strength for these super-tall buildings, inducing a good balance between drift and acceleration demands.

- The numerical and modelling outcome of this research may be immediately applied to design, vulnerability assessment and strengthening of super-tall mega-braced structures of similar type. In addition, the analysis framework prepared may be extended to other high-rise building classes and structural types, explicitly incorporating the contribution from further secondary systems such as slabs and facades, and may be integrated in a probabilistic approach for fragility analysis to become an effective tool for rational and quantitative risk assessment of super-tall frame-core structures that are prone to progressive collapse under seismic excitation.

References

[1] Fan H, Li QS, Tuan AY, Xu L. Seismic analysis of the world's tallest building. J Constr Steel Res 2009;65:1206–15.

[2] Lu X, Lu X, Guan H, Zhang W, Ye L. Earthquake-induced collapse simulation of a super-tall mega-braced frame-core tube building. J Constr Steel Res 2013;82:59–71.

[3] Lu X, Lu X, Sezen H, Ye L. Development of a simplified model and seismic energy dissipation in a super-tall building. Eng Struct 2014;67:109–22.

[4] Montuori GM, Mele E, Brandonisio G, De Luca A. Secondary bracing systems for diagrid structures in tall buildings. Eng Struct 2014;75:477–88.

[5] Montuori GM, Mele E, Brandonisio G, De Luca A. Geometrical patterns for diagrid buildings: exploring alternative design strategies from the structural point of view. Eng Struct 2014;71:112–27.

[6] Mele E, Toreno M, Brandonisio G, De Luca A. Diagrid structures for tall buildings: case studies and design considerations. Struct Des Tall Spec Build 2014;23:124–45.

[7] Montuori GM, Mele E, Brandonisio G, De Luca A. Design criteria for diagrid tall buildings: stiffness versus strength. Struct Des Tall Spec Build 2014;23:1294–314.

[8] Takewaki I, Murakami S, Fujita K, Yoshitomi S, Tsuji M. The 2011 off the Pacific coast of Tohoku earthquake and response of high-rise buildings under long-period ground motions. Soil Dyn Earthq Eng 2011;31:1511–28.

[9] Poursha M, Khoshnoudian F, Moghadam AS. A consecutive modal pushover procedure for estimating the seismic demands of tall buildings. Eng Struct 2009;31:591–9.

[10] Li QS, Zhang YH, Wu JR, Lin JH. Seismic random vibration analysis of tall buildings. Eng Struct 2004;26:1767–78.

[11] Meftah SA, Tounsi A, El Abbas AB. A simplified approach for seismic calculation of a tall building braced by shear walls and thin-walled open section structures. Eng Struct 2007;29:2576–85.

[12] Ji J, Elnashai AS, Kuchma DA. An analytical framework for seismic fragility analysis of RC high-rise buildings. Eng Struct 2007;29:3197–209.

[13] Khoshnoudian F, Kashani MMB. Assessment of modified consecutive modal pushover analysis for estimating the seismic demands of tall buildings with dual system considering steel concentrically braced frames. J Constr Steel Res 2012;72:155–67.

[14] Poursha M, Khoshnoudian F, Moghadam AS. A consecutive modal pushover procedure for nonlinear static analysis of one-way unsymmetric-plan tall building structures. Eng Struct 2011;33:2417–34.

[15] Jan TS, Liu MW, Kao YC. An upper-bound pushover analysis procedure for estimating the seismic demands of high-rise buildings. Eng Struct 2004;26:117–28.

[16] Searer G. Poorly worded, ill-conceived, and unnecessary code provisions. Struct Des Tall Spec Build 2006;15:533–46.

[17] Englekirk R. The impact of prescriptive provisions on the design of high-rise buildings. Struct Des Tall Spec Build 2005;14:455–64.

[18] Yang TY, Bozorgnia Y, Moehle JP. The tall buildings initiative. In: The 14th World Conference on Earthquake Engineering, Beijing, China, October 12–17, 2008.

[19] Li CS, Lam SSE, Zhang MZ, Wong YL. Shaking table test of a 1:20 scale high-rise building with a transfer plate system. J Struct Eng ASCE 2006;132:1732–44.

[20] Lu XL, Zou Y, Lu WS, Zhao B. Shaking table model test on Shanghai world financial center tower. Earthq Eng Struct Dyn 2007;36:439–57.

[21] Brunesi E, Nascimbene R. Extreme response of reinforced concrete buildings through fiber force-based finite element analysis. Eng Struct 2014;69:206–15.

[22] Brunesi E, Nascimbene R, Parisi F, Augenti N. Progressive collapse fragility of reinforced concrete framed structures through incremental dynamic analysis. Eng Struct 2015;104:65–79.

[23] OpenSees. Open system for earthquake engineering simulation. Berkeley (CA): Pacific Earthquake Engineering Research Center, University of California.

[24] Eurocode 8. Design of structures for earthquake resistance – Part 1: General rules, seismic actions and rules for buildings, EN 1998-1-1. Brussels (Belgium); 2005.

[25] Sullivan TJ. Direct displacement-based seismic design of steel eccentrically braced frame structures. Bull Earthq Eng 2013;11:2197–231.

[26] Maley TJ, Roldán R, Lago A, Sullivan TJ. Effects of response spectrum shape on the response of steel frame and frame-wall structures. Pavia (Italy): IUSS Press; 2012.

[27] Kim S, D'Amore E. Pushover analysis procedure in earthquake engineering. Earthq Spectra 1999;15:417–34.

[28] Krawinkler H, Seneviratna GDPK. Pros and cons of a pushover analysis of seismic performance evaluation. Eng Struct 1998;20:452–62.

[29] Chopra AK, Goel RK. A modal pushover analysis procedure for estimating seismic demands for buildings. Earthq Eng Struct Dyn 2002;31:561–82.

[30] Fajfar P. A nonlinear analysis method for performance based seismic design. Earthq Spectra 2000;16:573–92.

[31] Chopra AK, Goel RK. A modal pushover analysis procedure to estimate seismic demand for unsymmetric-plan buildings. Earthq Eng Struct Dyn 2004;33:903–27.

[32] Goel RK, Chopra AK. Evaluation of modal and FEMA pushover analysis: SAC buildings. Earthq Spectra 2004;20:225–54.

[33] Nascimbene R, Rassati GA, Wijesundara KK. Numerical simulation of gusset-plate connections with rectangular hollow section shape brace under quasi-static cyclic loading. J Constr Steel Res 2011;70:177–89.

[34] Santagati S, Bolognini D, Nascimbene R. Strain life analysis at low-cycle fatigue on concentrically braced steel structures with RHS shape braces. J Earthq Eng 2012;16:107–37.

[35] Brunesi E, Nascimbene R, Rassati GA. Response of partially-restrained bolted beam-to-column connections under cyclic loads. J Constr Steel Res 2014;97:24–38.

[36] Brunesi E, Nascimbene R, Rassati GA. Evaluation of the response of partially restrained bolted beam-to-column connection subjected to cyclic pseudo-static loads. Structures Congress 2013, Pittsburgh, Pennsylvania, May 2–4, 2013. p. 2310–21.

[37] Brunesi E, Nascimbene R, Rassati GA. Seismic response of MRFs with partially-restrained bolted beam-to-column connections through FE analyses. J Constr Steel Res 2015;107:37–49.

[38] Brunesi E, Nascimbene R, Rassati GA. Seismic performance of steel MRF with partially-restrained bolted beam-to-column connections through FE simulations. Structures Congress 2014, Boston, Massachusetts, April 3–5, 2014. p. 2640–51.

[39] Brunesi E, Bolognini D, Nascimbene R. Evaluation of the shear capacity of precast-prestressed hollow core slabs: numerical and experimental comparisons. Mater Struct 2015;48(5):1503–21.

[40] Brunesi E, Nascimbene R. Numerical web-shear strength assessment of precast prestressed hollow core slab units. Eng Struct 2015;102:13–30.

[41] Brunesi E, Nascimbene R, Pagani M, Beilic D. Seismic performance of storage steel tanks during the May 2012 Emilia, Italy, earthquakes. J Perform Constr Fac ASCE 2015;29(5):04014137.

[42] Brunesi E, Nascimbene R, Deyanova M, Pagani C, Zambelli S. Numerical simulation of hollow steel profiles for lightweight concrete sandwich panels. Comput Concr 2015;15(6):951–72.

[43] Yahia SA, Atmane HA, Houari MSA, Tounsi A. Wave propagation in functionally graded plates with porosities using various higher-order shear deformation plate theories. Struct Eng Mech 2015;53:1143–65.

[44] Bourada M, Kaci A, Houari MSA, Tounsi A. A new simple shear and normal deformations theory for functionally graded beams. Steel Compos Struct 2015;18:409–23.

[45] Tounsi A, Houari MSA, Benyoucef S, Adda Bedia EA. A refined trigonometric shear deformation theory for thermoelastic bending of functionally graded sandwich plates. Aerosp Sci Technol 2013;24:209–20.

[46] Zidi M, Tounsi A, Houari MSA, Adda Bedia EA, Anwar Bég O. Bending analysis of FGM plates under hygro-thermo-mechanical loading using a four variable refined plate theory. Aerosp Sci Tech 2014;34:24–34.

[47] Belabed Z, Houari MSA, Tounsi A, Mahmoud SR, Anwar Bég O. An efficient and simple higher order shear and normal deformation theory for functionally graded material (FGM) plates. Compos Part B – Eng 2014;60:274–83.

[48] Mahi A, Adda Bedia EA, Tounsi A. A new hyperbolic shear deformation theory for bending and free vibration analysis of isotropic, functionally graded, sandwich and laminated composite plates. Appl Math Model 2015;39: 2489–508.

[49] Bouderba B, Houari MSA, Tounsi A. Thermomechanical bending response of FGM thick plates resting on winkler-pasternak elastic foundations. Steel Compos Struct 2013;14:85–104.

[50] Bousahla AA, Houari MSA, Tounsi A, Adda Bedia EA. A novel higher order shear and normal deformation theory based on neutral surface position for bending analysis of advanced composite plates. Int J Comput Method 2014;11 (6):1350082.

[51] Hebali H, Tounsi A, Houari MSA, Bessaim A, Adda Bedia EA. New quasi-3D hyperbolic shear deformation theory for the static and free vibration analysis of functionally graded plates. J Eng Mech ASCE 2014;140:374–83.

[52] Meziane MAA, Abdelaziz HH, Tounsi A. An efficient and simple refined theory for buckling and free vibration of exponentially graded sandwich plates under various boundary conditions. J Sandwich Struct Mater 2014;16: 293–318.

[53] Khalfi Y, Houari MSA, Tounsi A. A refined and simple shear deformation theory for thermal buckling of solar functionally graded plates on elastic foundation. Int J Comput Methods 2014;11(5):135007.

[54] Larbi LO, Kaci A, Houari MSA, Tounsi A. An efficient shear deformation beam theory based on neutral surface position for bending and free vibration of functionally graded beams. Mech Based Des Struct Mach 2013;41:421–33.

[55] Rassati GA, Leon RT, Noè S. Component modeling of partially restrained composite joints under cyclic and dynamic loading. J Struct Eng ASCE 2004;130:343–51.

[56] Braconi A, Salvatore W, Tremblay R, Bursi OS. Behaviour and modelling of partial-strength beam-to-column composite joints for seismic applications. Earthq Eng Struct Dyn 2007;36:142–61.

[57] Latour M, Piluso V, Rizzano G. Cyclic modeling of bolted beam-to-column connections: component approach. J Earthq Eng 2011;15:537–63.

[58] Wijesundara KK, Nascimbene R, Sullivan TJ. Equivalent viscous damping for steel concentrically braced frame structures. Bull Earthq Eng 2011;9:1535–58.

[59] Wijesundara KK, Nascimbene R, Rassati GA. Modeling of different bracing configurations in multi-storey concentrically braced frames using a fiber-beam based approach. J Constr Steel Res 2014;101:426–36.

[60] Spacone E, Filippou FC, Taucer FF. Fibre beam-column model for non-linear analysis of RC frames: Part I. Formulation. Earthq Eng Struct Dyn 1996;25:711–25.

[61] SAP2000. Linear and nonlinear static and dynamic analysis and design of three-dimensional structures. Berkeley (CA): Computers and Structures Inc. (CSI).

[62] ASCE 7-05. Minimum design loads for buildings and others structures. Reston (VA): American Society of Civil Engineers; 2006.

[63] EN 10025-2. Hot rolled products of structural steels – Part 2: Technical delivery conditions for non-alloy structural steels. Brussels (Belgium); 2004.

[64] UNI EN 14399-1. High strength structural bolting assemblies or preloading – Part 1: General Requirements. Brussels (Belgium); 2005.

[65] Uriz P, Filippou FC, Mahin SA. Model for cyclic inelastic buckling for steel member. J Struct Eng ASCE 2008;134:619–28.

[66] Bai Y, Lin X. Numerical simulation on seismic collapse of thin-walled steel moment frames considering post local buckling behavior. Thin-Walled Struct 2015;94:424–34.

[67] Eurocode 3. Design of steel structures – Part 1-8: Design of joints, EN 1993-1-8, Brussels (Belgium); 2005.

[68] Ekh J, Schön J. Finite element modeling and optimization of load transfer in multi-fastener joints using structural elements. Compos Struct 2008;82:245–56.

[69] Swanson JA, Leon RT. Bolted steel connections: tests on T-stub components. J Struct Eng ASCE 2000;126:50–6.

[70] Scott MH, Fenves GL. Krylov subspace accelerated Newton algorithm: application to dynamic progressive collapse simulation of frames. J Struct Eng ASCE 2010;136:473–80.

[71] Priestley MJN, Grant DN. Viscous damping in seismic design and analysis. J Earthq Eng 2005;9:229–55.

[72] Kumar M, Stafford PJ, Elghazouli AY. Influence of ground motion characteristics on drift demands in steel moment frames designed to Eurocode 8. Eng Struct 2013;52:502–17.

[73] Kumar M, Stafford PJ, Elghazouli AY. Seismic shear demands in multi-storey steel frames designed to Eurocode 8. Eng Struct 2013;52:69–87.

[74] Shome N, Cornell CA, Bazzurro P, Carballo JE. Earthquakes, records, and nonlinear responses. Earthq Spectra 1998;14(3):469–500.

[75] Iervolino I, Cornell CA. Record selection for nonlinear seismic analysis of structures. Earthq Spectra 2005;21(3):685–713.

[76] Hancock J, Bommer JJ, Stafford PJ. Numbers of scaled and matched accelerograms required for inelastic dynamic analyses. Earthq Eng Struct Dyn 2008;37(14):1585–607.

[77] Faccioli E, Paolucci R, Rey J. Displacement spectra for long periods. Earthq Spectra 2004;20(2):347–76.

[78] Faccioli E, Villani M. Seismic hazard mapping for Italy in terms of broadband displacement response spectra. Earthq Spectra 2009;25(3):515–39.

[79] NEHRP. NEHRP (National Earthquake Hazard Reduction Program) recommended provisions for new buildings and other structures (FEMA P-750), 2009 ed. Washington (DC): Building Seismic Safety Council, National Institute of Building Sciences; 2009.

[80] NBCC. National Building Code of Canada (NBCC). Ottawa (Ontario, Canada): National Research Council Canada (NRCC); 1990.

[81] UBC. Uniform Building Code (UBC). Whittier (CA): International Council of Building Officials (ICBO); 1991.

[82] Uang CM. Establishing R (or Rw) and Cd factors for building seismic provisions. J Struct Eng ASCE 1991;117(1):19–28.

[83] Uang CM, Maarouf A. Deflection amplification factor for seismic design provisions. J Struct Eng ASCE 1994;120(8):2423–36.